AWARD NUMBER: W81XWH-13-1-0238

TITLE: Developing Inhibitors of Translesion DNA Synthesis as Therapeutic Agents against Lung Cancer

PRINCIPAL INVESTIGATOR: Anthony J. Bardis, Ph.D.

CONTRACTING ORGANIZATION: Cleveland State University
Cleveland, Ohio, 44115

REPORT DATE: December 2015

TYPE OF REPORT: Final

PREPARED FOR: U.S. Army Medical Research and Materiel Command
Fort Detrick, Maryland 21702-5012

REPORT DOCUMENTATION PAGE

Form Approved
OMB No. 0704-0188

1. REPORT DATE	2. REPORT TYPE	3. DATES COVERED
December 2015	Final	20Sep2013 - 19Sep2015

4. TITLE AND SUBTITLE

Developing Inhibitors of Translesion DNA Synthesis as Therapeutic Agents against Lung Cancer

5a. CONTRACT NUMBER

5b. GRANT NUMBER
W81XWH-13-1-0238

5c. PROGRAM ELEMENT NUMBER

6. AUTHOR(S)

Anthony J. Bardis, Ph.D.

E-Mail: a.berdis@csuohio.edu

5d. PROJECT NUMBER

5e. TASK NUMBER

5f. WORK UNIT NUMBER

7. PERFORMING ORGANIZATION NAME(S) AND ADDRESS(ES)

Cleveland State University
Cleveland, Ohio, 44115

8. PERFORMING ORGANIZATION REPORT NUMBER

9. SPONSORING / MONITORING AGENCY NAME(S) AND ADDRESS(ES)

U.S. Army Medical Research and Materiel Command
Fort Detrick, Maryland 21702-5012

10. SPONSOR/MONITOR'S ACRONYM(S)

11. SPONSOR/MONITOR'S REPORT NUMBER(S)

12. DISTRIBUTION / AVAILABILITY STATEMENT

Approved for Public Release; Distribution Unlimited

13. SUPPLEMENTARY NOTES

14. ABSTRACT

Oxygen-rich environments can create pro-mutagenic DNA lesions such as 8-oxoguanine (8-oxo-G) that can be misreplicated during translesion DNA synthesis (TLS). Our work has evaluated the pro-mutagenic behavior of 8-oxo- G by quantifying the ability of high-fidelity and specialized DNA polymerases to incorporate natural and modified nucleotides opposite this lesion. We have demonstrated that high-fidelity DNA polymerases (eukaryotic pol delta and bacteriophage T4 DNA polymerase) display error-prone tendencies when replicating 8-oxo-G, they display remarkably low efficiencies for TLS compared to normal DNA synthesis. In contrast, pol eta shows a combination of high efficiency and low fidelity when replicating 8-oxo-G. These combined properties are consistent with a pro- mutagenic role for pol eta when replicating this DNA lesion under cellular conditions. Studies with modified nucleotide analogs indicate that pol eta relies heavily on hydrogen-bonding interactions during normal and translesion synthesis. However, some nucleobase modifications including alkylation to the 06 and N2 position of guanine increase error-prone replication of 8-oxo-G. These results have identified two (2) nucleotide analogs that are efficiently and selectively utilized by pol eta. We tested the ability of the corresponding nucleoside analogs to act as anti-cancer agents by inhibiting the activity of pol eta when replicating damaged DNA induced by chemotherapeutic agents.

15. SUBJECT TERMS

Mutagenesls, DNA polymerases, nucleoslde analogs, chemotherapeutic agents

16. SECURITY CLASSIFICATION OF:			17. LIMITATION OF ABSTRACT	18. NUMBER OF PAGES	19a. NAME OF RESPONSIBLE PERSON
a. REPORT	b. ABSTRACT	c. THIS PAGE			USAMRMC
Unclassified	Unclassified	Unclassified	Unclassified	28	19b. TELEPHONE NUMBER *(include area code)*

Table of Contents

1. Introduction: This proposal set out to develop novel nucleoside and nucleotide analogs that possess both *thera*peutic and diag*nostic* activities against lung cancer. These "theranostic" nucleotides were designed to be efficiently and selectively utilized by several DNA polymerases that replicate damaged DNA. After incorporation, these analogs terminate the misreplication of damaged DNA to produce therapeutic effects against lung cancer. The ability to "tag" the nucleotides with fluorogenic moieties via "click" chemistry provides unique diagnostic capabilities to measure their incorporation opposite DNA lesions. The combined therapeutic and diagnostic activities will aid to define the role of pro-mutagenic DNA replication in the development and progression of lung cancer. By terminating the misreplication of damaged DNA, these analogs will help prevent DNA mutagenesis, an underlying cause of lung cancer. This last aspect provides the basis for a new therapeutic strategy against lung cancer that will combine these analogs with existing therapeutic agents that damage DNA. Toward this goal, we have identified two (2) lead nucleotides that are efficiently and selectively incorporated opposite a unique DNA lesion commonly formed under hyperoxic conditions present in the lung.

2. Keywords: Mutagenesis, lung cancer, DNA polymerases, nucleoside analogs, chemotherapeutic agents, chemosensitizers

3. Overall Project Summary:

Objective 1: Synthesis and testing of non-natural nucleotides against specialized DNA polymerases.

Task 1A. Synthesis of 5-substituted indolyl nucleosides and corresponding nucleotides.

We have completed the synthesis and chemical characterization of six (6) distinct nucleotide analogs using our established protocols. Provided below is the synthetic route for one compound designated 3-ethynyl-5-nitroindolyl-2'-deoxynucleoside (Figure 1).

Figure 1. Synthetic scheme for 3-ethynyl-5-nitroindolyl-2'-deoxynucleoside and corresponding nucleoside triphosphate.

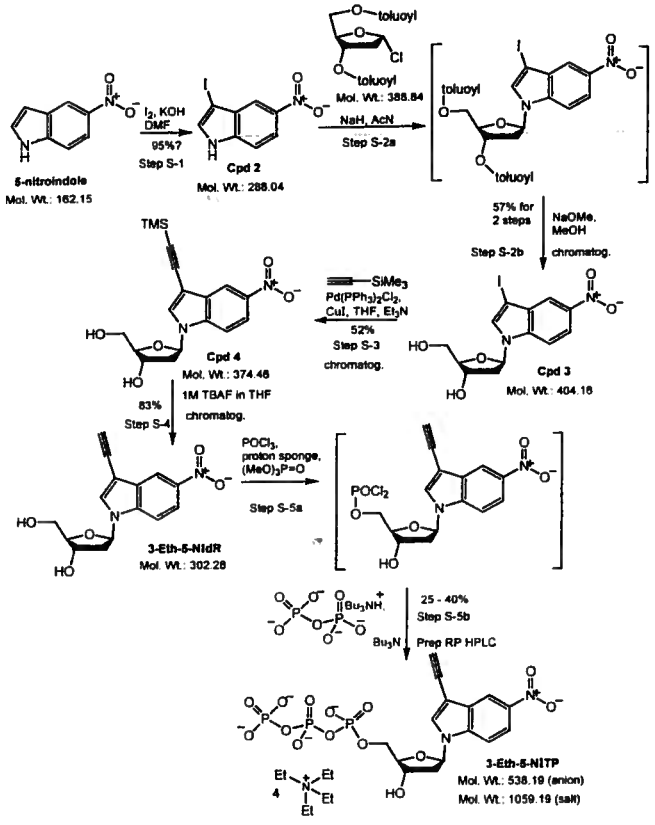

The identity of 3-ethynyl-5-nitroindolyl-2'-deoxynucleoside has been confirmed using LC/MS (liquid chromatography/mass spectroscopy) (Figure 2) and nuclear magnetic resonance (NMR spectroscopy (Figure 3).

Figure 2. Mass spectroscopy to verify the molecular weight of 3-ethynyl-5-nitroindolyl-2'-deoxynucleoside.

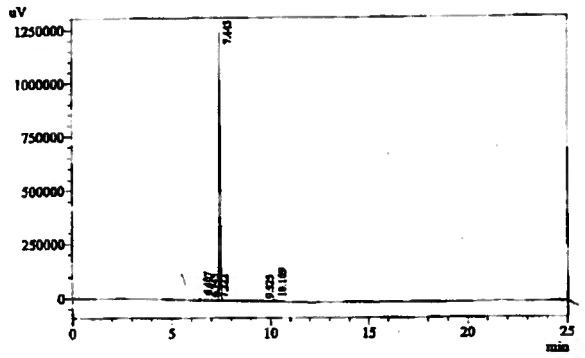

Figure 3. NMR spectrum of 3-ethynyl-5-nitroindolyl-2'-deoxynucleoside.

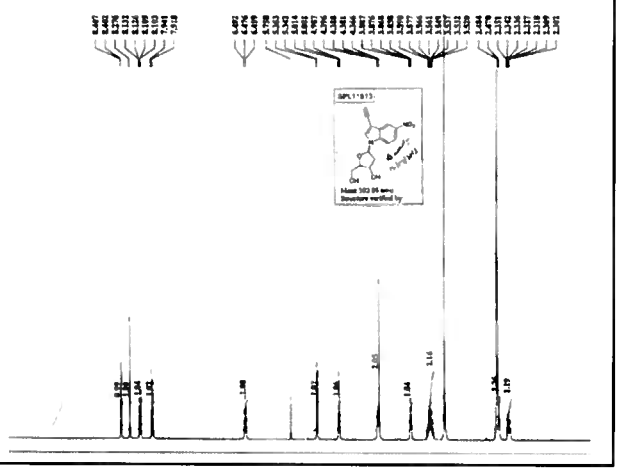

As described below, we have characterized the enzymatic incorporation of these analogs. Results of these studies have generated a structure-activity relationship to further develop additional analogs that are predicted to be both efficient and selective substrates for pol eta during the replication of oxidized DNA lesions. This task is complete.

Task 1B. Determination of Kinetic Parameters. k_{cat}, K_m, and k_{cat}/K_m values were measured for the aforementioned nucleotide analogs developed in ***Task 1A***. Figures 4 and 5 provides representative Michaelis-Menten plots for the utilization of dATP and N^2-MedGTP during the replication of the oxidized lesion, 8-oxoguanine (8-oxoG) catalyzed by human pol eta (pol η). These kinetic data

Figure 4. Michaelis-Menten plot for the incorporation of dATP opposite 8-oxoguanine (8-oxoG) catalyzed by human pol eta.

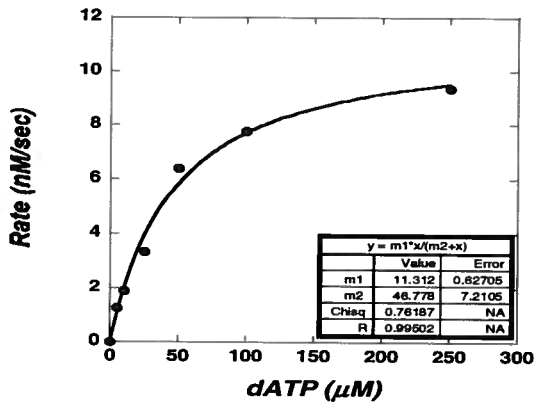

Figure 5. Michaelis-Menten plot for the incorporation of N^2-MedGTP opposite 8-oxoguanine (8-oxoG) catalyzed by human pol eta.

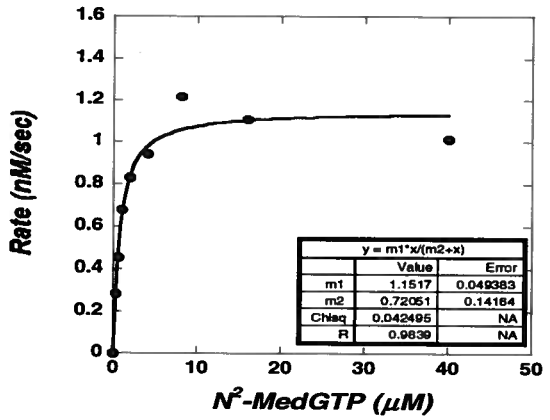

In addition, we measured the kinetic parameters for ten (10) other analogs, several of which were previously synthesized in my laboratory. The kinetic parameters for these analogs are summarized in Tables 1 and 2.

Table 1. Summary of kinetic constants measured for the incorporation of natural and modified nucleotides opposite 8-oxoguanine (8-oxo-G) by pol η.

Nucleotide	K_m (μM)	k_{cat} (sec^{-1})	k_{cat}/K_m ($M^{-1}sec^{-1}$)	Efficiency
dATP	47 +/- 7	1.13 +/- 0.06	(2.4 +/- 0.3)*10^4	100%
N^6-MedATP	46 +/- 15	1.35 +/- 0.15	(2.9 +/- 0.2)*10^4	120%
6-Cl-PTP	137 +/- 7	0.39 +/- 0.08	(2.8 +/- 0.4)*10^3	12%
6-Cl-2APTP	14.3 +/- 3.2	0.09 +/- 0.01	(6.3 +/- 0.6)*10^3	26%
dGTP	32 +/- 10	0.25 +/- 0.03	(7.8 +/- 0.8)*10^3	33%
O^6-MedGTP	50 +/- 15	0.55 +/- 0.13	(1.1 +/- 1.0)*10^4	46%
N^2-MedGTP	**0.64 +/- 0.05**	**0.11 +/- 0.02**	**(1.7 +/- 0.1)*10^5**	**720%**

Table 2. Summary of kinetic constants measured for the incorporation of non-natural nucleotides opposite g 8-oxoguanine by polymerase eta.

Nucleotide	K_m (μM)	k_{cat} (sec^{-1})	k_{cat}/K_m ($M^{-1}sec^{-1}$)	Efficiency
dATP	47 +/- 7	1.13 +/- 0.06	24,000 +/- 3,000	100%
IndTP	61 +/- 18	0.050 +/- 0.005	820 +/- 120	3.4%
5-MeITP	18 +/- 5	0.047 +/- 0.001	2,610 +/- 200	10.9%
5-EtITP	36 +/- 16	0.007 +/- 0.001	200 +/- 50	0.8%
5-EyITP	56 +/- 36	0.0015 +/- 0.0003	27 +/- 15	0.1%
5-NITP	63 +/- 12	0.344 +/- 0.020	5,460 +/- 550	23%
4-NITP	23 +/- 8	0.132 +/- 0.016	5,740 +/- 350	24%
6-NITP	**3.9 +/- 1.6**	**0.283 +/- 0.032**	**72,600 +/- 1,200**	**303%**

These studies have identified two (2) lead compounds highlighted in **bold** that show promising activity as selective and efficient substrates for pol eta. These analogs, N^2-MedGTP and 6-NITP, are incorporated opposite 8-oxoguanine several-fold more efficiently than dATP. As described below, we are in the process of testing the efficacy of the corresponding nucleoside analogs to inhibit pol eta activity under cellular conditions. These studies will ultimately define the potential anti-cancer activities of the nucleoside analogs against lung cancer. Finally, a manuscript describing the results of these studies has been published in the scientific journal "*Nucleic Acids Research*". This task is complete.

Task 1C. Evaluating Chain Termination Capabilities. We have investigated the ability of several non-natural nucleotides studied in this project to function as chain-terminating substrates for various DNA polymerases. Representative gel electrophoresis data is provided in Figure 5 and shows interesting results that highlight the ability of pol η to perform pro-mutagenic DNA synthesis when replicating 8-oxo-G. As illustrated, pol η can easily extend beyond dCMP and dAMP when paired opposite 8-oxo-G. An interesting feature is that pol η easily extends beyond dAMP even in

the absence of the next correct nucleotide. This is unusual as this specialized polymerase appears to misinsert dATP opposite A at position 15 of the template. When supplied with the nucleotides needed for elongation, pol η again easily extends beyond both mispaired primers/templates to yield full length product.

Figure 6. Gel electrophoresis data summarizing the incorporation and extension of modified and non-natural nucleotides opposite 8-oxo-G catalyzed by pol eta.

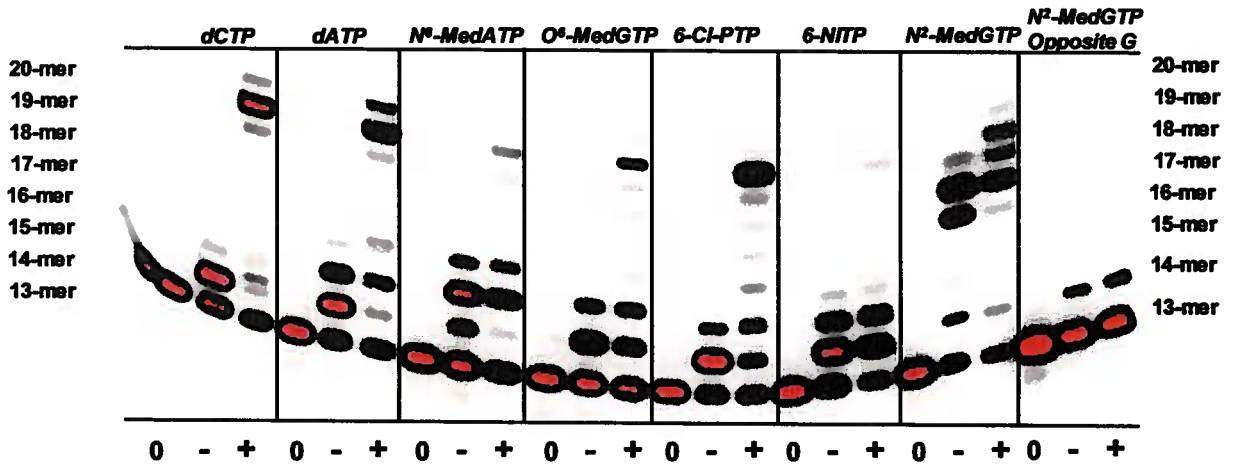

Similar results are obtained when pol η is supplied with modified nucleotides. In particular, pol η easily elongates beyond 6-Cl-PTP, N^6-MedATP, and O^6-MedGTP in the absence of the next correct nucleotide. However, slight differences are observed in the efficiency of elongation when supplied with nucleotides needed for complete elongation of the primer. In this case, the halogenated analog, 6-Cl-PTP is elongated with a higher efficiency compared to either of the alkylated nucleotides, N^6-MedATP and O^6-MedGTP.

6-NITP is incorporated opposite 8-oxo-G and subsequently extended in the absence of complementary dNTPs. However, pol η poorly extends beyond 6-NIMP when supplied with the next correct nucleotides, dTTP and dGTP. This later result is consistent with previous reports demonstrating that high-fidelity DNA polymerases display difficulties in elongating substituted indolyl-nucleotides. Thus, our in vitro data indicates that 6-NITP functions as an efficient chain-terminating nucleotide for pol η. However, the most unusual behavior is that exhibited by N^2-MedGTP. Specifically, pol η efficiently inserts N^2-MedGTP opposite 8-oxo-G and continues to elongate the mispair to positions 17 and 18 of the template. Thus, pol η effectively misinserts N^2-MedGTP opposite a templating adenine (A) and then incorporates opposite two templating cytosine (C) bases before terminating synthesis at the next templating adenine (A). This task is complete.

Task 1D. Utilization by Other DNA Polymerases. We have measured the kinetic parameters (k_{cat}, K_m, and k_{cat}/K_m) for the aforementioned nucleotide analogs developed in **Task 1A** using several different DNA polymerases including high fidelity DNA polymerases such as pol δ. Our results summarized below in Tables 3 and 4 indicate that most of our nucleotide analogs behave as poor substrates for high fidelity DNA polymerases involved in chromosomal DNA replication. This validates our conclusion that several of these analogs are selective for the specialized DNA polymerase, pol eta, during the replication of oxidized DNA lesions. This task is complete.

Table 3. Summary of kinetic parameters for the incorporation of modified nucleotides opposite 8-oxoguanine.

dNTP	K_m [μM]	k_{cat} [sec^{-1}]	k_{cat}/K_m [M^{-1} sec^{-1}]	Efficiency
dATP	566 ± 25	0.535 ± 0.015	$1.03 * 10^3$	100 %
2,6-APTP	1,370 ± 410	0.787 ± 0.156	$0.5 * 10^3$	50 %
dITP	28 ± 8	0.008 ± 0.005	$2.9 * 10^2$	27 %
6-Cl-PTP	51 ± 17	0.0123 ± 0.0007	$2.31 * 10^2$	15 %
6-Cl-2APTP	145 ± 33	0.049 ± 0.004	$3.37 * 10^2$	22 %
dGTP	*No insertion*			NA
N^6-MedATP	135 ± 41	0.056 ± 0.005	$4.14 * 10^2$	18 %
O^6-MedGTP	82 ± 11	0.023 ± 0.001	$2.79 * 10^2$	19 %
N^2-MedGTP	*No insertion*			NA

Table 4. Summary of kinetic parameters for the incorporation of non-natural nucleotides opposite 8-oxoguanine.

dNTP [μM]	K_m [μM]	k_{cat} [sec^{-1}]	k_{cat}/K_m [M^{-1} sec^{-1}]	Efficiency
dATP	566 ± 25	0.535 ± 0.015	$1.5 * 10^3$	100 %
5-MeITP	260 ± 98	0.042 ± 0.008	$1.62 * 10^2$	11 %
5-EtITP	184 ± 36	0.079 ± 0.007	$4.3 * 10^2$	29 %
5-EyITP	41.3 ± 9.2	0.030 ± 0.002	$7.14 * 10^2$	48 %
4-NITP	28 ± 10	0.052± 0.004	$1.84 * 10^3$	122 %
6- NITP	53 ± 13	0.097 ± 0.008	$1.82 * 10^3$	122 %
5-NITP	264 ± 31	0.036 ± 0.002	$1.34 * 10^2$	9%

Objective 2: Biological testing of non-natural nucleosides against lung cancer cell lines.

Task 2A. To evaluate the function of non-natural nucleosides as anti-cancer agents. We have measured the dose-dependency of the corresponding non-natural deoxyribosides developed under Objective 1. Specifically, IC_{50} and LD_{50} values are being measured against the following cell lines: A549, ACC-LC-48, AA8pIK8, and H69AR. Cell viability and growth are assessed via routine MTT assays using a microplate reader. Figure 7 provides a representative dose response curve for the anti-cancer effects of one of our non-natural nucleosides, 5-NIdR, against the A549 cell line. Note that we tested this specific analog first as we previously demonstrated using leukemia cells (MOLT4 and CEM-C7) as well as adherent cells (HCT116 (colon), U87 (glioblastoma), and fibroblasts) that 5-NIdR displays low potency when used as a monotherapeutic agent. The data presented here recapitulates this result. However, 5-NIdR works synergistically with certain DNA damaging agents such as temozolomide which produces non-instructional lesions such as abasic sites. We are currently testing the ability of 5-NIdR and other modified nucleoside analogs to work in combination with therapeutic agents which create reactive oxygen species and that are likely to generate DNA lesions such as 8-oxoguanine. In addition, we are assessing cell viability and cell growth via microscopy studies (data not shown). This task is complete.

Figure 7. Dose response curve for the anti-cancer effects of 5-NIdR against the lung cancer cell line, A549.

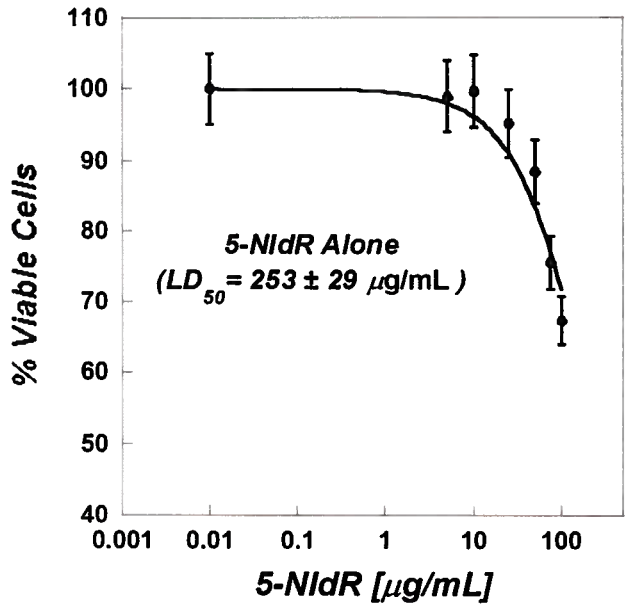

Task 2B. To Evaluate the Mechanism of Cell Death. Flow-cytometry studies are planned over the next six (6) months to investigate the mechanism of cell death induced by the corresponding non-natural nucleoside analogs. The primary technique is propidium iodide and annexin V staining to differentiate between apoptosis versus necrosis. Figure 8 provides representative plots from dual parameter flow cytometry experiments examining the anti-cancer effects of 5-NIdR against the A549 cell line. These data demonstrate that treatment with 100 mg/mL of 5-NIdR alone does produce a significant increase in apoptosis compared to cells treated with DMSO (vehicle control).

Figure 8. Dual parameter flow cytometry measuring the anti-cancer effects of DMSO versus 5-NIdR against the A549 cell line.

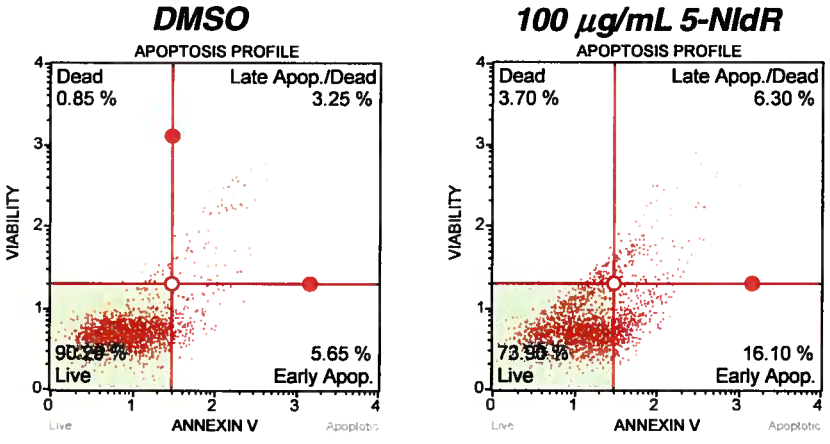

Our original hypothesis was that combining 5-NIdR and DNA damaging agents that create miscoding lesions similar to 8-oxoguanine should generate a synergistic increase in apoptosis. We tested this hypothesis by treating cancer cells with 5-NIdR alone and in combination with low doses of temozolomide, a DNA damaging agent that preferentially reacts with guanine residues in DNA to create two distinct lesions, O^6-methylguanine and abasic sites. Both lesions can inhibit DNA synthesis which subsequently induces cell death. Both lesions can be misreplicated in a process called translesion DNA synthesis that can limit the efficacy of temozolomide by causing drug resistance and increasing mutagenesis. Figure 9 provides representative plots from dual parameter flow cytometry experiments comparing the effects of temozolomide alone, 5-NIdR alone, and cells treated with a combination of temozolomide and 5-NIdR. It is clear that a significantly higher level of apoptosis is observed in cells treated with the combination of agents compared to treatment with either compound individually. This result is consistent with our initial hypothesis.

Figure 9. Results of dual parameter flow cytometry experiments demonstrating the ability of 5-NIdR to increase the cell-killing effects of DNA damaging agents.

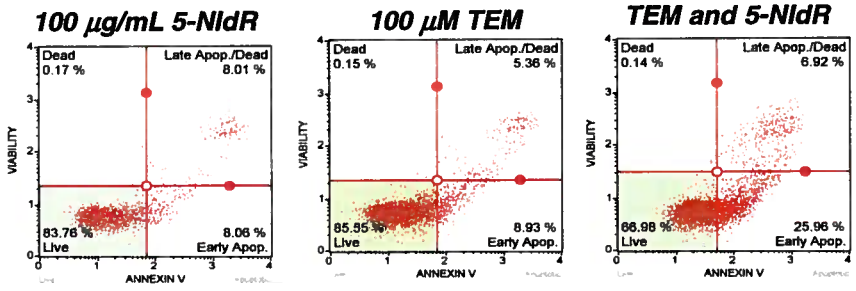

We next used the DNA Damage Response Assay from EMD Millipore to quantitatively measure single-strand and double-strand DNA breaks in cells treated with temozolomide and 5-NIdR. Single-strand DNA causes ATM phosphorylation and while double-strand DNA breaks result in H2AX phosphorylation. The level of these phosphorylated proteins accurately reflects the amount of cellular DNA damage. Cancer cells were treated with DMSO, temozolomide, 5-NIdR, and temozolomide combined with 5-NIdR. After 72 hours, cells were stained with antibodies directed against pH2AX and pATM. Representative data provided in Figure 10 show that cells treated with temozolomide combined with 5-NIdR show higher levels of pATM and pH2AX compared to treatment with TEM or 5-NIdR. The increase in pATM levels is indicative of high levels of single strand DNA that result from inhibiting DNA synthesis during S-phase. Collectively, the results from these biochemical studies confirm that 5-NIdR potentiates the cell killing effects of DNA damaging agents by inhibiting the ability of DNA polymerases to replicate DNA lesions that are produced by temozolomide.

Figure 10. The combination of temozolomide and 5-NIdR generates higher levels of pATM and pH2AX compared to treatment with TEM or 5-NIdR.

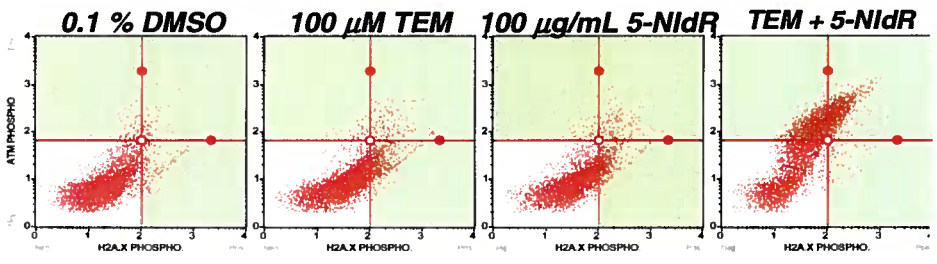

Task 2C. siRNA Knockdown Experiments to Identify Specialized DNA Polymerases Involved in Utilizing Non-Natural Nucleosides. siRNA knockdown experiments were planned to target various specialized DNA polymerase such as polymerase eta, iota, and kappa that are involved in replicating damaged DNA. Our kinetic data obtained under ***Task 1B*** indicates that pol eta may be

the primary polymerase responsible for misreplcating oxidized DNA lesions such as 8-oxoguanine. Unfortunately, we were unable to complete these experiments as funding expired.

Objective 3: Validating the diagnostic applications of therapeutic nucleoside analogs.

Task 3A. *In vitro* validation assays. *In vitro* "clicking" reactions were performed using our published protocols to verify that the non-natural nucleotides could function as effective diagnostic probes to detect the replication of damaged DNA. As expected, all of the non-natural nucleotides developed here function as diagnostic probes. However, there are some differences in the overall efficiencies for the "clicking" reactions that range from 45-75% efficiency. This task is complete.

Task 3B. Validation of Diagnostic Applications by Cell-Based Studies. In situ "clicking" reactions were performed using the nucleoside analogs developed in Objective 1. These studies were initially delayed by technical issues. Despite these delays, we were able to use high-filed microscopy to visualize the activity of our "clickable" nucleoside inside cancer cells. In these experiments, cancer cells were treated with DMSO or 10 μg/mL 3-Eth-5-NIdR in the absence and presence of a sub-lethal dose of temozolomide. After 3 days of treatment, cells were trypsinized and harvested by centrifugation and washed with PBS to remove 3-Eth-5-NIdR and/or 3-Eth-5-NITP not incorporated into DNA. After fixation and permeabilization, the cells were treated with AlexaFluor488-azide and Cu(I) catalyst to covalently attach the fluorogenic probe to 3-Eth-5-NITP incorporated into DNA. Prior to microscopy analysis, cells were co-stained with DAPI to identify the nucleus. Microscopy images provided in Figure 14 show that cells treated with 100 μM temozolomide and 10 μg/mL 3-Eth-5-NIdR show high levels of green fluorescence which co-localizes within the nucleus (panel D). These results suggest that generating abasic sites by treating with temozolomide allows for increased levels of 3-Eth-5-NITP to be stably inserted into genomic DNA. In the absence of exogenous DNA damage, 3-Eth-5-NIdR is poorly incorporated into genomic DNA (data not show).

Figure 14. Microscopic images provide evidence that 3-Eth-5-NIdR is incorporated opposite DNA generated by temozolomide treatment.

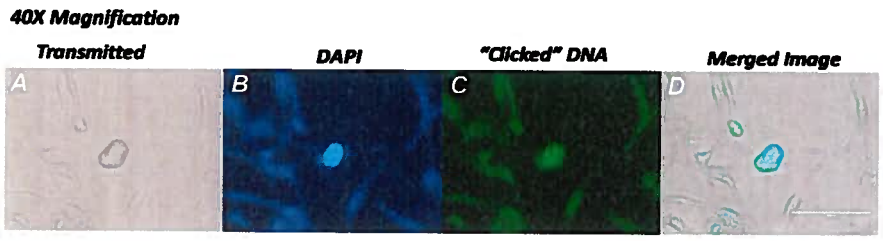

As described under Objective 1, we characterized two lead non-natural nucleotides, N^2-MedGTP & 6-NITP, which function as effective substrates for polymerase eta during the replication of oxidized DNA lesions including 8-oxoguanine. Unfortunately, we were unable to pursue cell based studies examining their potential therapeutic and diagnostic activities as the funding period for this proposal expired and funds from other funding agencies have not let been obtained to complete this work.

4. Key Research Accomplishments:

- Completed the synthesis and chemical characterization of six (6) distinct nucleotide analogs.
- Measured the incorporation of sixteen (16) distinct nucleotide analogs opposite 8-oxo-guanine, a miscoding DNA lesion associated with lung cancer.
- Identified two (2) nucleotide analogs that are efficiently and selectively incorporated opposite 8-oxo-guanine.
- Demonstrated that one nucleotide analog functions as a chain-terminating substrate for pol eta.
- Tested the biological activity of these analogs against several lung cell lines including A549, ACC-LC-48, AA8pIK8, and H69AR.
- Demonstrated the ability of a non-natural nucleoside to increase the cell-killing effects of a DNA damaging agent.
- Acceptance of a manuscript entitled "The use of modified and non-natural nucleotides provide unique insights into the pro-mutagenic replication catalyzed by polymerase eta." in Nucleic Acids Research. (Choi JS, Dasari A, Hu P, Benkovic SJ, Berdis AJ. The use of modified and non-natural nucleotides provide unique insights into pro-mutagenic replication catalyzed by polymerase eta. Nucleic Acids Res. 2016 Feb 18;44(3):1022-35. doi: 10.1093/nar/gkv1509. Epub 2015 Dec 29. PubMed PMID: 26717984; PubMed Central PMCID: PMC4756837.

5. Conclusion:

More people in the United States die from lung cancer than any other type of cancer. The development and progression of lung cancer is in most cases directly linked to mutagenesis caused by the misreplication of damaged DNA. Our research funded by the Department of Defense has provided new insight into this process. In this respect, we have identified several novel nucleotide analogs that function as effective DNA polymerase substrates when replicating DNA lesions associated with lung cancer. These analogs have provided a deeper understanding of the molecular mechanisms for lung cancer development as well as acquired resistance to treatment with DNA damaging agents. Perhaps more importantly, these analogs are being used to develop an innovative strategy for treating early stage lung cancer. Finally, our studies are applying these analogs as predictive and prognostic markers to identify non-responders of chemotherapeutic agents that cause DNA damage.

6. Publications, Abstracts, and Presentations:

Publication: Choi, J.S., Dasari, A., Hu, P., Benkovic, S.J., and Berdis, A.J. The use of modified and non-natural nucleotides provide unique insights into pro-mutagenic replication catalyzed by polymerase eta. Nucleic Acids Res. 2016 Feb 18;44(3):1022-35. doi: 10.1093/nar/gkv1509. Epub 2015 Dec 29. PubMed PMID: 26717984; PubMed Central PMCID: PMC4756837.

Presentations:

1.) Anvesh Dasari and Anthony J. Berdis. "Evaluating the Pro-Mutagenic replication of 8-oxoguanine." 19th Annual Buffalo DNA Replication and Repair Symposium, Buffalo New York (June 19th, 2015)

2.) Jung-Suk Choi, Casey Seol Kim, and Anthony J. Berdis. Pharmacological and Pre-Clinical testing of 5-NIdR as a New Therapeutic Agent Against Cancer" 19th Annual Buffalo DNA Replication and Repair Symposium, Buffalo New York (June 19th, 2015)

3.) Jung-Suk Choi, Casey Seol Kim, and Anthony J. Berdis. "Inhibiting translesion DNA synthesis as a strategy to hinder pathoadaptation and drug resistance." 14th International Conference on the Chemistry of Antibiotics and other Bioactive Compounds, Galveston Texas. (October 13-16, 2015)

7. Inventions, Patents, and Licenses: None to date

8. Reportable Outcomes: None to date

9. Other Achievements: None to date

10. References: ***N/A***

11. Appendices: See attached manuscript

1022–1035 Nucleic Acids Research, 2016, Vol. 44, No. 3
doi: 10.1093/nar/gkv1509

Published online 29 December 2015

The use of modified and non-natural nucleotides provide unique insights into pro-mutagenic replication catalyzed by polymerase eta

Jung-Suk Choi[1], Anvesh Dasari[1], Peter Hu[2], Stephen J. Benkovic[2] and Anthony J. Berdis[1,3,4,*]

[1]Department of Chemistry, Cleveland State University, 2351 Euclid Avenue, Cleveland, OH 44115, USA, [2]Department of Chemistry, The Pennsylvania State University, 413 Wartik Building, University Park, PA 16802, USA, [3]Center for Gene Regulation in Health and Disease, Cleveland State University, 2351 Euclid Avenue, Cleveland, OH 44115, USA and [4]Case Comprehensive Cancer Center, 10900 Euclid Avenue, Cleveland OH 44106, USA

Received September 24, 2014; Revised November 23, 2015; Accepted December 10, 2015

ABSTRACT

This report evaluates the pro-mutagenic behavior of 8-oxo-guanine (8-oxo-G) by quantifying the ability of high-fidelity and specialized DNA polymerases to incorporate natural and modified nucleotides opposite this lesion. Although high-fidelity DNA polymerases such as pol δ and the bacteriophage T4 DNA polymerase replicating 8-oxo-G in an error-prone manner, they display remarkably low efficiencies for TLS compared to normal DNA synthesis. In contrast, pol η shows a combination of high efficiency and low fidelity when replicating 8-oxo-G. These combined properties are consistent with a pro-mutagenic role for pol η when replicating this DNA lesion. Studies using modified nucleotide analogs show that pol η relies heavily on hydrogen-bonding interactions during translesion DNA synthesis. However, nucleobase modifications such as alkylation to the N2 position of guanine significantly increase error-prone synthesis catalyzed by pol η when replicating 8-oxo-G. Molecular modeling studies demonstrate the existence of a hydrophobic pocket in pol η that participates in the increased utilization of certain hydrophobic nucleotides. A model is proposed for enhanced pro-mutagenic replication catalyzed by pol η that couples efficient incorporation of damaged nucleotides opposite oxidized DNA lesions created by reactive oxygen species. The biological implications of this model toward increasing mutagenic events in lung cancer are discussed.

INTRODUCTION

DNA replication is the biological process in which an organism's genome is copied by the action of at least one DNA polymerase. The vast majority of DNA polymerases use the coding information present on the templating strand of DNA (or RNA) to guide each nucleotide incorporation event. The efficiency and fidelity of this process are often attributed to the formation of complementary hydrogen-bonding interactions that define a correct base pair (1,2). The mutual recognition of adenine (A) by thymine (T) and of guanine (G) by cytosine (C) involves complementarity in shape, size and hydrogen-bonding interactions made between each base pair. Using these interactions, most replicative DNA polymerases synthesize DNA with an incredible degree of fidelity, making only 1 mistake every million opportunities (3) at remarkably high speeds of >500 bp/s (4).

While the molecular mechanism of normal DNA synthesis is well understood, our knowledge of how DNA polymerases replicate damaged DNA is far less defined. Much of this deficiency arises from two major complications. These first involves the diversity of DNA lesions formed inside the cell while the second reflects the number of DNA polymerases that can replicate each lesion. For example, there are over a hundred different DNA lesions that can form within a cell (5), and many of these lesions can drastically influence DNA polymerase activity (6). For instance, lesions which significantly alter the proper conformation of the DNA template such as abasic sites and thymine dimers are strong replication blocks for most high-fidelity DNA polymerases (7–9). If left unrepaired, these types of lesions would constantly interrupt DNA synthesis catalyzed by high-fidelity DNA polymerases and produce devastating effects on cell proliferation and viability. To avoid catastrophic failures caused by damaged DNA, prokaryotic and eukaryotic cells possess several 'specialized' DNA polymerases that can efficiently replicate vari-

*To whom correspondence should be addressed. Tel: +1 216 687 2454; Fax: +1 216 687 9298; Email: a.berdis@csuohio.edu

ous DNA lesions. The ability of DNA polymerases to bypass damaged DNA is a process termed translesion DNA synthesis (TLS) and can result in error-free or error-prone replication. Although error-prone activity during TLS can reduce genomic fidelity, it is essential as most cells would die without the ability of specialized DNA polymerases to efficiently replicate unrepaired DNA lesions.

However, not all forms of DNA damage produce such dire effects on the efficiency of DNA replication. In fact, many DNA lesions have simple alterations to the hydrogen-bonding potential of the nucleobase that can enhance pro-mutagenic replication (10–12). At the cellular level, this increase in mutagenic DNA synthesis is a hallmark of several hyperproliferative diseases such as cancer. Indeed, lung cancer represents an important example as the oxygen-rich environment of the lung can produce reactive oxygen species (ROS) that can generate promutagenic DNA lesions such as 2,6-diamino-4-hydroxy-5-formamidopyrimidine (faPyG) and 8-oxo-guanine (8-oxo-G) (Figure 1A). Since both lesions are miscoding, they can be replicated in an error-free or error-prone manner (13,14). For example, 8-oxo-G can be replicated incorrectly via the incorporation of adenosine-2′-deoxyriboside monophosphate (dAMP), leading to an overall increase in G:C to T:A transversion mutations. At the molecular level, the misreplication of 8-oxo-G depends upon the *syn*- versus *anti*-conformation of the oxidized nucleobase (Figure 1B). Error-free replication occurs when cytosine-2′-deoxyriboside monophosphate (dCMP) is inserted opposite the *anti*-conformation of 8-oxo-G. In contrast, promutagenic synthesis occurs when dAMP insertion opposite the *syn*-conformation of 8-oxo-G which resembles thymine with respect to hydrogen-bonding interactions. A number of laboratories have performed kinetic and structural studies with different DNA polymerases to define the replication of 8-oxo-G (15–22). In general, the results from these studies demonstrate that the efficiency and selectivity for inserting dCMP versus dAMP opposite 8-oxoG varies significantly depending on which DNA polymerase is used as well as the context of DNA sequence. For example, studies with high-fidelity DNA polymerases from different sources demonstrate an unusual preference for misinserting dAMP opposite the oxidized DNA lesion compared to the correct partner, dCMP (15–17). In contrast, studies with various specialized DNA polymerases have yielded conflicting results. For example, Dpo4, the error prone DNA polymerase from *Sulfolobus solfataricus* is reported to catalyze error-free replication of 8-oxo-G (18). In contrast, human pol κ is more proficient at catalyzing error-prone synthesis when replication 8-oxo-G (19). In addition, several studies have compared the activity of pol η isolated from yeast or human cells. Carlson and Washington demonstrated that pol η can efficiently incorporate dAMP opposite 8-oxo-G (20). Likewise, McCulloch *et al.* showed that yeast pol η replicates 8-oxo-G more accurately than its high-fidelity counterpart, pol δ (21). Finally, Patra *et al.* reported that human pol η replicates 8-oxo-G in a predominantly error-free manner by preferentially inserting dCMP (22).

To better understand the molecular mechanisms of TLS and induced-mutagenesis, we compared the abilities of high-fidelity and specialized DNA polymerases to replicate 8-oxo-G. Our quantitative analyses demonstrate that the incredible efficiency of high-fidelity DNA polymerases for replicating normal DNA is reduced ~1000-fold when replicating the oxidized lesion, 8-oxo-G. This reduction in efficiency suggests that these polymerases are unlikely to replicate this miscoding lesion under physiological conditions. Consistent with this model, the specialized DNA polymerase, pol η, replicates 8-oxo-G approximately 100-fold more efficiently than either high-fidelity DNA polymerase. In addition, pol η misinserts dAMP opposite 8-oxo-G with a catalytic efficiency comparable to dCMP insertion. The combination of high efficiency and promiscuity for misinserting dAMP likely contributes to the mutagenic potential of the oxidized DNA lesion. Furthermore, we identified a specific nucleotide, N^2-MedGTP, which is unique in its utilization and selectivity by pol η when replicating 8-oxo-G. This result suggests that inappropriate modifications to DNA and nucleotide pools can cause a synergistic increase in pro-mutagenic DNA synthesis. The biological ramifications of these findings are discussed in the context of disease models such as lung cancer in which increased levels of ROS can enhance disease development and progression.

MATERIALS AND METHODS

Materials

[γ–^{32}P]-ATP was purchased from MP Biomedical (Irvine, CA, USA). Unlabeled deoxynucleoside triphosphate (dNTPs) (ultrapure) were obtained from Pharmacia. Unlabeled dNTPs (ultrapure) were obtained from Pharmacia. Magnesium acetate, magnesium chloride and Trizma base were from Sigma. Urea, acrylamide and bis-acrylamide were from National Diagnostics (Rochester, NY, USA). Oligonucleotides, including those containing 8-oxo-guanine, were synthesized by Operon Technologies (Alameda, CA, USA). All modified nucleotides including N^6-MedATP, 6-Cl-PTP, 6-Cl-2APTP, O^6-MedGTP, N^2-MedGTP, 2-6-dATP, dITP and 8-oxo-dGTP were obtained from Trilink Biotechnologies (San Diego, CA, USA). All non-natural nucleotides including IndTP, 5-MeITP, 5-Et-ITP, 5-EyITP, 5-NITP, 4-NITP and 6-NITP were synthesized and purified as previously reported (23–26). All other materials were obtained from commercial sources and were of the highest available quality. Exonuclease-deficient bacteriophage T4 DNA polymerase (gp43exo$^-$ (Asp-219 to Ala mutation)) was purified and quantified as previously described (27). Recombinant human polymerase delta (pol δ) and human polymerase eta (pol η) were purified as previously described (28,29). All DNA polymerases used in this study were >97% pure as assessed by sodium dodecylsulphate-polyacrylamide denaturing gel electrophoresis.

Kinetic parameters for nucleotide incorporation

Kinetic studies using the bacteriophage T4 DNA were performed using an assay buffer consisting of TrisOAc (25 mM pH 7.5), KOAc (150 mM), DTT (10 mM) and 10 mM MgAcetate at pH 7.5. Kinetic studies using polymerase δ and η were performed using an assay buffer consisting of TrisOAc (50 mM pH 7.5), bovine serum albumin (1 mg/ml),

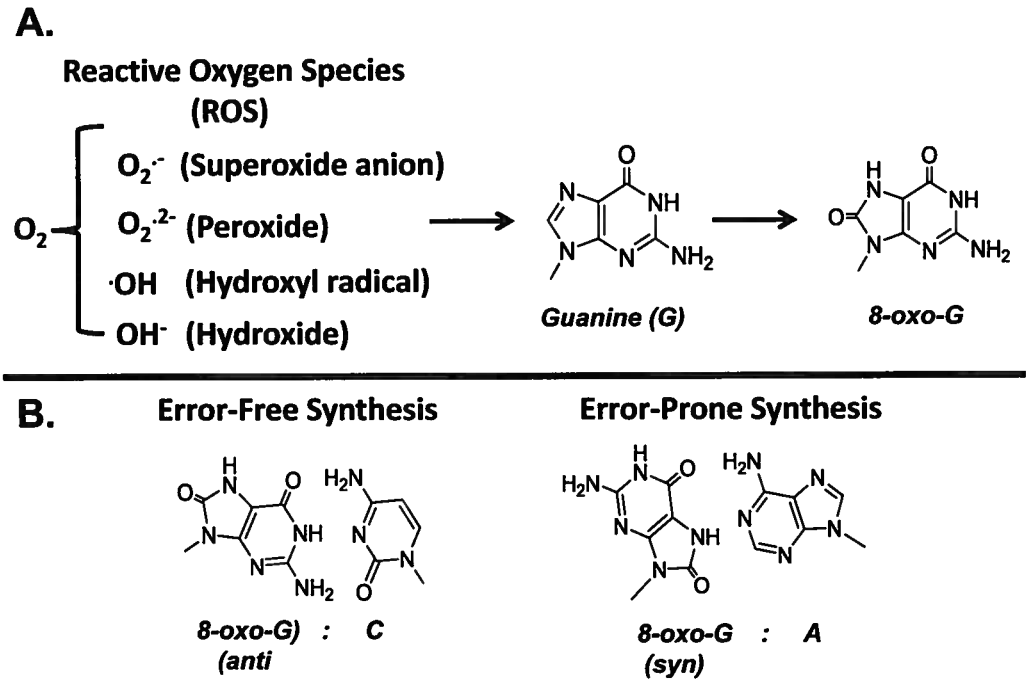

Figure 1. (A) Overview describing the ability of reactive oxygen species (ROS) to modify natural nucleobases such as guanine to generate miscoding DNA lesions such as 8-oxo-guanine (8-oxo-G). (B) The replication of 8-oxo-guanine can be error-free via dCMP insertion or error-prone via dAMP insertion.

DTT (10 mM) and 5 mM $MgCl_2$ at pH 7.5. All assays were performed at 25°C unless otherwise noted. The kinetic parameters (k_{cat}, K_m and k_{cat}/K_m) for nucleotides were measured as previously described (30). Briefly, a typical assay was performed by pre-incubating DNA substrate (500 nM) with a limiting amount of polymerase (10 or 25 nM) in assay buffer and Mg^{2+}. Reactions were initiated by adding variable concentrations of nucleotide substrate (1–500 μM). At variable time intervals, 5 μl aliquots of the reaction were quenched by adding an equal volume of 200 mM ethylenediaminetetraacetic acid (EDTA). Polymerization reactions were monitored by analyzing products on 20% sequencing gels as previously described (29). Gel images were obtained with a Packard PhosphorImager by using the OptiQuant software supplied by the manufacturer. Product formation was quantified by measuring the ratio of ^{32}P-labeled extended and un-extended primer. The ratios of product formation are corrected for substrate in the absence of polymerase (zero point). Corrected ratios are then multiplied by the concentration of primer/template used in each assay to yield total product. Steady-state rates were obtained from the linear portion of the time course and were fit to Equation (1)

$$y = mx + b \quad (1)$$

where m is the slope of the line corresponding to the rate of the polymerization reaction (nM s^{-1}), b is the y-intercept and t is time. Data for the dependency of rate as a function of nucleotide concentration were fit to the Michaelis–Menten equation (Equation 2):

$$v = V_{max} * [dNTP]/(K_m + [dNTP]) \quad (2)$$

where v is the rate of product formation (nM s^{-1}), V_{max} is the maximal rate of polymerization, K_m is the Michaelis constant for dXTP and [dXTP] is the concentration of nucleotide substrate. The turnover number, k_{cat}, is V_{max} divided by the final concentration of polymerase used in the experiment.

Extension beyond 8-oxo-guanine

Single turnover conditions were used to measure extension beyond various mispairs containing 8-oxo-G in the template. Pol η (500 nM) was incubated with 250 nM DNA (13/20OG-mer) in assay buffer and mixed with a fixed concentration of nucleotide substrate and 5 mM $MgCl_2$. In all cases, the concentration of nucleotide was maintained at its respective K_m value. An aliquot of the reaction was quenched with 500 mM EDTA after 60 or 120 s (time to achieve 4 half-lives as calculated from k_{cat} values). This time point represents insertion opposite the DNA lesion. An aliquot containing 200 μM of dTTP and dGTP was then added to initiate elongation beyond the formed mispair. After an additional 60 s, an aliquot of the reaction was quenched. Products of the polymerization reactions were processed and analyzed as described above to define the efficiency of elongation.

Molecular modeling studies

Crystal structures containing putative structural models of pol η in complex with DNA template containing 8-oxo-G were obtained from the Research Collaboratory for Structural Bioinformatics Protein Data Bank (www.pdb.org).

The structural models of pol η containing $DNA_{8\text{-}og}$–dNTP complex were made from the co-crystal structure of pol η-$DNA_{8\text{-}og}$–dATP/dCTP (PDB ID and 403R/403S) (22). Pol η is structurally and functionally homologous in both the crystal structures.

Using the molecular modeling program, *Molecular Operating Environment*, modified dNTP structures for N^2-MedGMP and 6-NIMP were created by modifying dAMP in the crystal structure PDB ID: 403R. Following the modifications, the active site of pol η was minimized using MOE modeling software (MOE 2014). The molecular modeling program *Chimera* was used to determine interglycosyl distances and distance between the templating base and active amino residues using the modified structural model of Pol η-$DNA_{8\text{-}og}$–N^2MeGMP/6-NIMP. Hydrophobicity surface models were generated for the polymerase containing DNA and dNTP using the Kyle Doolittle hydrophobicity scale. The scale of hydrophobicity is represented in decreasing order as Red>White>Blue.

RESULTS

Comparison of normal and translesion DNA synthesis activity catalyzed by high-fidelity and specialized DNA polymerases

This study begins by comparing the ability of two high fidelity DNA polymerases (bacteriophage T4 DNA polymerase (gp43 exo$^-$) and human pol δ) and a specialized DNA polymerase (human pol η) to incorporate natural dNTPs opposite normal and damaged nucleobases. Defined DNA substrates containing G, C or 8-oxo-G at position 14 of the template (Figure 2A) were used to accurately quantify the activity of each DNA polymerase. Denaturing gel electrophoresis images provided in Figure 2B illustrate the ability of these DNA polymerases to perform normal synthesis (dCMP insertion opposite G), incorrect synthesis (dAMP insertion opposite G) and TLS (dCMP or dAMP insertion opposite 8-oxo-G). During normal replication, both high-fidelity polymerases are remarkably faithful as they insert dCMP opposite G much more efficiently than dAMP. However, gp43 exo$^-$ and pol δ exhibit pro-mutagenic tendencies by efficiently incorporating dAMP opposite 8-oxo-G. In contrast, the specialized polymerase, pol η, displays less fidelity when replicating undamaged DNA, a results that is consistent with previous reports (31,32). Furthermore, pol η displays more promiscuous behavior when replicating 8-oxo-G as dATP and dCTP are utilized with nearly equal efficiencies. This result is consistent with work performed by Carlson and Washington (20) and McCulloch *et al.* (21) showing that pol η utilizes dATP with high efficiency when replicating 8-oxo-G.

To more accurately assess the kinetic behavior of these polymerases, k_{cat}, K_m and k_{cat}/K_m values were measured for the insertion of dCTP and dATP opposite G and 8-oxo-G. Figure 2C provides Michaelis–Menten plots for dCMP incorporation opposite G while Figure 2D provides Michaelis–Menten plots for dCMP incorporation opposite 8-oxo-G catalyzed by gp43 exo$^-$. The kinetic parameters for gp43 exo$^-$ during normal and TLS are summarized in Table 1. As expected, gp43 exo$^-$ displays a high catalytic efficiency of $1.7 * 10^5$ $M^{-1}s^{-1}$ during normal DNA synthesis, and this is achieved by a relatively low K_m value of 4.7 μM for dCTP and a fast k_{cat} value of 0.94 s^{-1}. In contrast, the catalytic efficiency for replicating 8-oxo-G decreases by ~20-fold, and this reflects a 10-fold increase in the K_m for dCTP coupled with a 2-fold reduction in k_{cat}. Surprisingly, the efficiency for dAMP insertion opposite 8-oxo-G is only 4-fold lower than dCMP (compare k_{cat}/K_m values of 3000 $M^{-1}s^{-1}$ for dATP versus 11 000 $M^{-1}s^{-1}$ for dCTP). This effect is caused exclusively by a large increase in the K_m value for dATP (compare K_m values of 54 versus 250 μM for dCTP and dATP, respectively).

Identical experiments performed using pol δ, the high-fidelity human DNA polymerase, yield the kinetic parameters for normal and TLS summarized in Table 1. These data indicate that pol δ is also highly proficient during normal DNA synthesis, displaying a low K_m of 0.64 μM and a fast k_{cat} of 1 s^{-1} for incorporating dCMP opposite G. Similar to gp43 exo$^-$, the efficiency for replicating 8-oxo-G is reduced significantly as the K_m for dCTP and k_{cat} are both adversely affected. In particular, the K_m for dCTP is 50-fold higher than that measured during normal DNA synthesis while the k_{cat} value is reduced ~30-fold when replicating the oxidized lesion. This later result indicates that the rate-limiting step for polymerase turnover is sensitive to the nature of the DNA lesion, and this represents an interesting difference between pol δ and gp43exo$^-$ when replicating 8-oxo-G that is currently being investigated.

The kinetic parameters for pol η are considerably different than both high-fidelity DNA polymerases. As summarized in Table 1, the K_m value for dCTP is only 2-fold higher when replicating the oxidized DNA leison (compare 1.3 versus 3.0 μM for G and 8-oxo-G, respectively). Likewise, the k_{cat} value during TLS is only 2-fold lower than for replicating normal DNA (compare 0.40 s^{-1} versus 0.88 s^{-1} for 8-oxo-G and G, respectively). Collectively, these data demonstrate that pol η misinserts dAMP opposite 8-oxo-G with a high catalytic efficiency of 24 000 $M^{-1}s^{-1}$. In fact, the value measured for pol η is 60-fold higher than that measured for the efficiency of pol δ misinserting dAMP opposite 8-oxo-G. Since catalytic efficiencies are often used as predictors for enzyme activity *in vivo*, our results suggest that pol η is more proficient at catalyzing error-prone replication of 8-oxo-G compared to pol δ under cellular conditions.

Quantifying the incorporation of modified nucleotide analogs by Pol η

Several models have been proposed to explain why pol η displays promiscuous and low replicative fidelity, especially when replicating normal or undamaged DNA (33–37). One generalized model invokes the contributions of hydrogen-bonding interactions made between the incoming nucleotide with the templating nucleobase and/or with amino acids residing within the polymerase's active site (33–37). An alternative model suggests that pol η possesses a 'loose' active site that is larger than most high-fidelity DNA polymerases and thus capable of better accommodating DNA lesions (38). The concept that the relative 'tightness' of the active site of a DNA polymerase was predicated on work initially described by Kool *et al.* demonstrating that base analogs such as 2,4-difluorotoluene which lack classi-

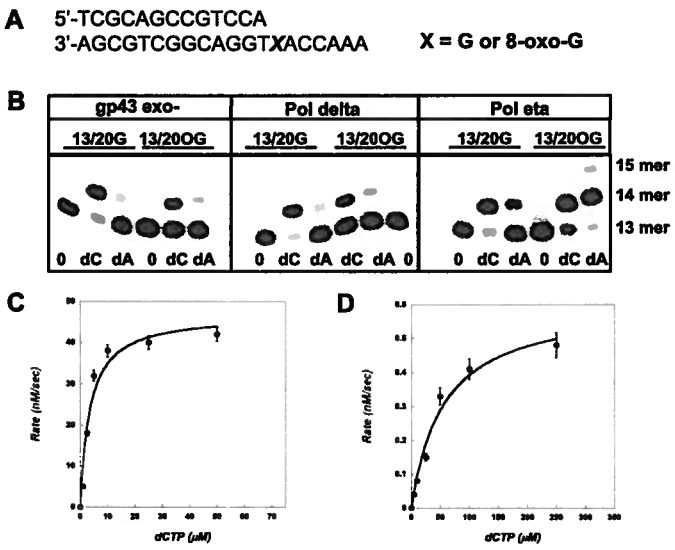

Figure 2. (A) DNA substrate used in these studies. X in the template at position 14 denotes G, C or 8-oxo-G. (B) Denaturing gel electrophoresis images comparing dCMP insertion opposite G (13/20G) and the insertion of dCMP and dAMP insertion opposite 8-oxo-G (13/20OG) by the bacteriophage T4 DNA polymerase, pol δ and pol η. (C) Michaelis–Menten plots for dCMP incorporation opposite G catalyzed by the bacteriophage T4 polymerase. (D) Michaelis–Menten plots for dCMP incorporation opposite 8-oxo-G catalyzed by the bacteriophage T4 polymerase.

Table 1. Summary of kinetic constants for the incorporation of natural nucleotides opposite guanine and 8-oxo-guanine by the bacteriophage T4 DNA polymerase (gp43 exo$^-$), pol δ and pol η

DNA	dNTP	K_m (μM)	k_{cat} (s^{-1})	k_{cat}/K_m ($M^{-1}s^{-1}$)
T4 DNA polymerase				
13/20G	dCTP	4.7 ± 0.1	0.94 ± 0.02	(1.7 ± 0.1)*10^5
13/20G	dATP	ND	ND	ND
13/20OG	dCTP	54 ± 16	0.59 ± 0.07	(1.1 ± 0.4)*10^4
13/20OG	dATP	250 ± 40	0.76 ± 0.13	(3.0 ± 0.3)*10^3
Pol δ				
13/20G	dCTP	0.64 ± 0.07	1.03 ± 0.02	(1.6 ± 0.5)*10^6
13/20G	dATP	ND	ND	ND
13/20OG	dCTP	34 ± 5	0.033 ± 0.002	(9.8 ± 0.4)*10^3
13/20OG	dATP	258 ± 14	0.097 ± 0.003	(0.4 ± 0.1)*10^3
Pol η				
13/20G	dCTP	1.3 ± 0.3	0.88 ± 0.10	(6.7 ± 0.3)*10^5
13/20G	dATP	49 ± 13	1.11 ± 0.08	(2.2 ± 0.4)*10^4
13/20OG	dCTP	3.0 ± 0.6	0.40 ± 0.02	(1.3 ± 0.1)*10^5
13/20OG	dATP	47 ± 7	1.13 ± 0.06	(2.4 ± 0.3)*10^4

cal hydrogen-bonding groups are efficiently and selectively incorporated opposite natural nucleobases such as adenine (39). This suggested that the shape of the formed base pair rather than H-bonding interactions serve as the primary source for nucleotide selection and incorporation by DNA polymerases.

To further investigate these mechanisms, we quantified the incorporation of several distinct purine nucleoside triphosphates that contain alterations to hydrogen-bonding functional groups (Figure 3A). We classified these modified nucleotides into three distinct groups. The first includes alkylated nucleotides such as N^6-MedGTP, O^6-MedGTP and N^2-MedGTP that were used to evaluate the contributions of hydrogen-bonding interactions, shape complementarity/steric fit and nucleobase hydrophobicity. The second group includes analogs in which a hydrogen-bonding group is replaced with a halogen (6-Cl-dATP and 6-Cl-2APTP). These substitutions provide a way to more accurately evaluate the contributions of shape complementarity/steric fit and nucleobase hydrophobicity. The final group are purines in which hydrogen-bonding groups are removed (dITP) or added (2,6-dATP) to more directly interrogate the contributions of hydrogen-bonding interactions.

Figure 3B provides representative Michaelis–Menten plots comparing the utilization of dATP with N^6-MedATP and 6-Cl-PTP when replicating 8-oxo-G. Surprisingly, alkylation at the N6-position of dATP actually causes a slight increase in the catalytic efficiency for insertion opposite 8-oxo-G compared to the natural substrate, dATP. In this case, the K_m of 46 μM for N^6-MedATP is identical to dATP ($K_m = 47$ μM) whereas the k_{cat} value for N^6-MedATP is increased slightly (compare 1.35 s^{-1} versus 1.13 s^{-1} for N^6-MedATP and dATP, respectively). At face value, this result

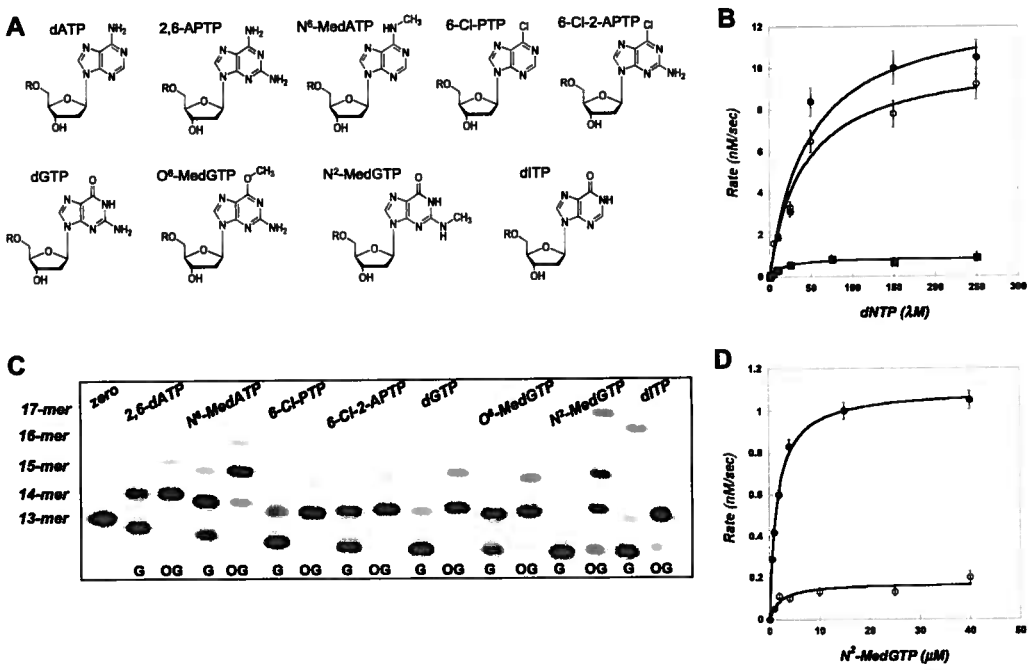

Figure 3. (A) Structures of modified purine nucleotides used in this study. (B) Michaelis–Menten plots comparing the utilization of dATP (○), N^6-MedATP (•) and 6-Cl-PTP (■) during the replication of 8-oxo- G catalyzed by polymerase η. (C) Gel electrophoresis data comparing the incorporation of modified natural nucleotides opposite G and 8-oxo-G catalyzed by pol eta. G represents guanine while OG represents 8-oxoguanine. (D) Michaelis–Menten plots for the insertion of N^2-MedGTP opposite G (○) and 8-oxo-G (•) catalyzed by polymerase eta.

suggests that altering hydrogen-bonding interactions has a minimal effect of the activity of pol η. However, data obtained with the halogenated analog, 6-Cl-PTP, suggests otherwise. In fact, replacing a hydrogen-bonding group (-NH_2) with a halogen (non-hydrogen bonding group) lowers the overall catalytic efficiency by producing negative effects on both K_m and k_{cat}. As summarized in Table 2, the reduced efficiency for utilizing 6-Cl-PTP is caused by a 3-fold increase in K_m coupled with a 3-fold decrease in k_{cat}. Similar results are obtained for the majority of nucleotide analogs tested here as modification to one or more hydrogen-bonding groups present on the incoming nucleotide causes a reduction in incorporation efficiencies (Table 2). For example, the catalytic efficiencies for 6-Cl-2APTP and O^6-MedGTP are lower than dATP for insertion opposite 8-oxo-G, suggesting that hydrogen bonding groups are indeed needed to optimize pol η activity when replicating 8-oxo-G. However, the position of the hydrogen bonding group also appears critical as analogs such as 2,6-dATP and ITP have lower incorporation efficiencies compared to dATP. Indeed, 8-oxo-dGTP displays the lowest activity amongst the substrates tested here as its catalytic efficiency is 50-fold lower than dATP and 16-fold lower than dGTP. This reduction is likely caused by alterations in the *anti-* versus *syn*-conformation of the nucleotide (40).

Surprisingly, there is one remarkable instance in which modifications to a hydrogen-bonding group actually causes a substantial increase in nucleotide utilization during the replication of 8-oxo-G. Specifically, N^2-MedGTP is utilized ~10- and 20-fold more effectively than dATP and dGTP, respectively. This increase in utilization occurs via a large enhancement in the K_m value for N^2-MedGTP rather than an effect on k_{cat}. In this case, the K_m of 0.64 μM for N^2-MedGTP is 70-fold lower that dATP (K_m = 47 μM) whereas the k_{cat} value for N^2-MedGTP is 10-fold lower (compare 0.11 s^{-1} versus 1.13 s^{-1} for N^2-MedGTP and dATP. This represents an unusual case as the K_m values for the majority of modified nucleotides tested here are either identical or are slightly higher than dATP. In fact, the K_m value for most analogs tested here remains fairly constant at ~50 μM while the k_{cat} value is the kinetic parameter that varies more significantly amongst these modified analogs.

To verify that these effects are not limited to TLS, we also measured if these modifications affect the efficiency of replicating undamaged DNA. As illustrated in Figure 3C, as pol η inserts most modified nucleotides opposite 8-oxo-G much more efficiently than opposite unmodified G. To verify that the preferential utilization occurs only during TLS, we measured the kinetic parameters for their incorporation opposite G. As summarized in Table 2, the catalytic efficiencies for most modified analogs are ~10- to 100-fold lower during normal synthesis compared to the replication of 8-oxo-G. In most cases, these reductions are caused by reductions in k_{cat} rather than through perturbations in the K_m. Collectively, these kinetic data indicate that modifications to a natural dNTP can increase the efficiency in the error-prone replication of 8-oxo-G catalyzed by pol η. However, these modifications do not significantly affect the fidelity of pol η when replicating undamaged DNA. Again, N^2-MedGTP represents the best example of this phenomenon as it displays a ~40-fold higher selectivity for insertion opposite 8-oxo-G than G (Figure 3D and Table 2). The greater selectivity of

Table 2. Summary of kinetic constants measured for the incorporation of natural and modified nucleotides opposite guanine (G) and 8-oxoguanine (8-oxo-G) by pol η

Nucleotide	K_m (μM)	k_{cat} (s^{-1})	k_{cat}/K_m ($M^{-1}s^{-1}$)	Efficiency[a]	Selectivity[b]
13/20OG					
dATP	47 ± 7	1.13 ± 0.06	(2.4 ± 0.3)*10^4	100%	1.14
N^6-MedATP	46 ± 15	1.35 ± 0.15	(2.9 ± 0.2)*10^4	120%	2.23
6-Cl-PTP	137 ± 7	0.39 ± 0.08	(2.8 ± 0.4)*10^3	12%	8.48
6-Cl-2APTP	14.3 ± 3.2	0.09 ± 0.01	(6.3 ± 0.6)*10^3	26%	1.26
dGTP	32 ± 10	0.25 ± 0.03	(7.8 ± 0.8)*10^3	33%	1.04
O^6-MedGTP	50 ± 15	0.55 ± 0.13	(1.1 ± 1.0)*10^4	46%	17.2
N^2-MedGTP	0.64 ± 0.05	0.11 ± 0.02	(1.7 ± 0.1)*10^5	720%	41
2,6-dATP	72 ± 19	0.31 ± 0.01	(4.3 ± 0.5)*10^3	18%	11.9
dITP	64 ± 25	0.17 ± 0.03	(2.7 ±0.9)*10^3	11%	5.6
8-oxo-dGTP	143 ± 36	0.068 ± 0.005	(4.8 ± 0.8)*10^2	2%	2.5
13/20G					
dATP	49 ± 13	1.11 ± 0.08	(2.2 ± 0.4)*10^4	100%	
N^6-MedATP	70 ± 30	0.88 ± 0.01	(1.3 ± 0.5)*10^3	6%	
6-Cl-PTP	77 ± 16	0.025 ± 0.001	(3.3 ± 0.9)*10^2	1.5%	
6-Cl-2APTP	15.9 ± 3.9	0.08 ± 0.01	(5.0 ± 0.8)*10^3	23%	
dGTP	2.4 ± 0.9	0.018 ± 0.001	(7.5 ± 0.9)*10^3	34%	
O^6-Me-dGTP	150 ± 70	0.096 ± 0.017	(6.4 ± 0.8)*10^2	2.9%	
N^2-Me-dGTP	5.5 ± 2.1	0.023 ± 0.004	(4.2 ± 0.8)*10^3	19%	
2,6-dATP	76 ± 17	0.027 ± 0.002	(3.6 ± 0.8)*10^2	1.6%	
dITP	25 ± 4	0.012 ± 0.001	(4.8 ± 06)*10^2	2.2%	
8-oxo-dGTP	183 ± 41	0.035 ± 0.003	(1.9 ± 0.5)*10^2	0.9%	

N^2-MedGTP for damaged DNA, coupled with its 10-fold higher catalytic efficiency, highlights a pro-mutagenic role for pol η during the replication of damaged DNA.

Incorporation of 5-substituted indolyl nucleotide analogs by Pol η

To further evaluate the role of hydrogen-bonding, shape complementarity and hydrophobicity, we quantified the incorporation of a series of 5-substituted indolyl-2′-deoxynucleotide analogs depicted in Figure 4A. Data provided in Figure 4B shows the ability of pol η to incorporate these nucleoside analogs opposite 8-oxo-G. The kinetic parameters for these analogs are summarized in Table 3 and reveal that these 5-substituted indolyl-2′-deoxynucleotide analogs are poor substrates for pol η. Specifically, the catalytic efficiencies for these indolyl-based nucleotides are between 5- to 1000-fold lower than dATP. This decrease efficiency is caused primarily by reductions in k_{cat} rather than through significant perturbations in K_m. The effect on k_{cat} values again suggest that the rate-limiting step for pol η turnover is highly sensitive to proper hydrogen bonding interactions made between the templating nucleobase with the incoming dNTP. While these data suggest that hydrogen-bonding interactions are important for the polymerization cycle, they also point to a role for steric fit during TLS. This is evident as the overall size of the incoming nucleotide influences the catalytic efficiency of nucleotide utilization. Figure 4C provides molecular models highlighting how the overall shape and size of the incoming nucleobase can influence its kinetic behavior. For example, 5-MeITP, a good pairing partner for the *syn*-conformation of 8-oxo-G, possesses a k_{cat}/K_m that is 3-fold higher than the smaller analog, IndTP. Furthermore, the k_{cat}/K_m decreases as the size of the incoming nucleotide increases beyond an optimal interglycosyl distance of 10.6 Å for a normal Watson–Crick base pair. In particular, the k_{cat}/K_m for 5-EtITP is 10-fold lower than that for 5-MeITP while that for 5-EyITP is 100-fold lower than 5-MeITP. This later result is interesting as 5-EtITP and 5-EyITP are similar in size. Thus, the reduction in catalytic efficiency likely reflects the influence of entropy on nucleotide utilization by pol η. In this case, the conjugated double bond present on 5-EyITP reduces rotational freedom of the functional group, and this entropic penalty could diminishes its utilization as a substrate. Consistent with this mechanism, 5-NITP displays the highest catalytic efficiency amongst all 5-substituted indolyl-nucleotides tested here. We argue that rotational freedom of the nitro group improves its efficiency for incorporation. However, other features such as increased pi-electron density associated with the nitro moiety may also play a role as this has been previously demonstrated for high-fidelity DNA polymerases when replicating non-instructional DNA lesions (41,42).

The denaturing gel provided in Figure 4B also compares the incorporation of these non-natural nucleotides opposite G versus 8-oxo-G. Visual inspection reveals that most analogs are preferentially incorporated opposite 8-oxo-G as they are poorly inserted opposite G. The kinetic parameters summarized in Table 3 confirm that the efficiency for their incorporation opposite G is lower, thus indicating that they are also poor substrates for pol η during normal DNA synthesis.

The position of the nitro moiety influences the efficiency and selectivity for incorporation

Previous work in our lab demonstrated that the position of the nitro moiety on the indole-nucleotide influences the selectivity for utilization by high fidelity DNA polymerase

Table 3. Summary of kinetic constants measured for the incorporation of non-natural nucleotides opposite guanine and 8-oxoguanine by polymerase η

Nucleotide	K_m (μM)	k_{cat} ($^{-1}$)	k_{cat}/K_m ($M^{-1}s^{-1}$)	Efficiency	Selectivity
13/20OG					
dATP	47 ± 7	1.13 ± 0.06	24 000 ± 3000	100%	1.09
IndTP	61 ± 18	0.050 ± 0.005	820 ± 120	3.4%	3.0
5-MeITP	18 ± 5	0.047 ± 0.001	2610 ± 200	10.9%	11.6
5-EtITP	36 ± 16	0.007 ± 0.001	200 ± 50	0.8%	0.24
5-EyITP	56 ± 36	0.0015 ± 0.0003	27 ± 15	0.1%	0.075
5-NITP	63 ± 12	0.344 ± 0.020	5460 ± 550	23%	0.30
4-NITP	23 ± 8	0.132 ± 0.016	5740 ± 350	24%	8.57
6-NITP	3.9 ± 1.6	0.283 ± 0.032	72 600 ± 1200	303%	1.80
13/20G					
dATP	49 ± 13	1.11 ± 0.08	22 000 ± 4000	100%	
IndTP	81 ± 18	0.022 ± 0.001	270 ± 80	1.2%	
5-MeITP	40 ± 15	0.009 ± 0.12	225 ± 80	1.0%	
5-EtITP	10 ± 3	0.008 ± 0.001	830 ± 100	3.8%	
5-EyITP	26 ± 5	0.009 ± 0.001	360 ± 50	1.6%	
5-NITP	46 ± 15	0.83 ± 0.12	18 000 ± 1200	82%	
4-NITP	57 ± 18	0.038 ± 0.009	670 ± 150	3.0%	
6-NITP	2.7 ± 0.6	0.108 ± 0.008	40 000 ± 1500	180%	

during the replication of normal and damaged DNA (26). Here, we tested if pol η shows similar behavior by preferentially utilizing one of these nitro-containing nucleotides during normal or TLS.

The kinetic parameters for the utilization of 4-NITP, 5-NITP and 6-NITP by pol η are summarized in Table 3. Close inspection reveals that pol η utilizes 4-NITP with an identical catalytic efficiency compared to 5-NITP when replicating 8-oxo-G. However, the K_m for 4-NITP is ~2.5-fold lower than 5-NITP while the k_{cat} for 4-NITP is 2.5-fold lower than 5NITP. Surprisingly, 6-NITP is a very efficient substrate for pol η as the k_{cat}/K_m for 6-NITP is 13-fold higher than either 4-NITP or 5-NITP and 3-fold greater than dATP. In all cases, the higher catalytic efficiency for 6-NITP is caused exclusively by a 15-fold decrease in its K_m value while the k_{cat} value is similar to the other substituted indolyl-nucleotides. While 6-NITP is highly efficient for insertion opposite 8-oxo-G, it displays only a 2-fold preference for the oxidized lesion compared to G. A more interesting effect is observed with 4-NITP as it displays a ~10-fold higher selectivity for incorporation opposite 8-oxo-G compared to G. Much of this selectively arises as 4-NITP is poorly utilized by pol η when replicating undamaged DNA. Collectively, these data demonstrate that the efficiency and selectivity of substrate utilization by pol η can be influenced by permutations in the position of the nitro moiety.

Extension beyond 8-oxo-guanine

The mutagenic potential of a DNA lesion depends not only upon which nucleotide is misinserted opposite it but also by the ability of the polymerase to elongate beyond the formed mispair. As such, we explored the ability of pol η to extend beyond two natural nucleotides (dCMP and dAMP), three modified purines (N^6-MedAMP, O^6-MedGMP and N^2-MedGMP), and one substituted indolyl nucleotide (6-NIMP) after they are incorporated opposite 8-oxo-G. These specific nucleotides were chosen as they are efficiently inserted opposite the oxidized lesion. Protocols outlined in Figure 5A were used to measure the ability of pol η to insert and extend various nucleotides opposite 8-oxo-G. Assays were performed using single turnover reaction conditions in order to maximize signal-to-noise ratios in product formation. Under these conditions, pol η (500 nM) and 13/20OG-mer (250 nM) were pre-incubated in assay buffer and then mixed with a fixed concentration of nucleotide (dNTP) and 5 mM Mg^{2+} to initiate insertion opposite the lesion. After four half-lives, an aliquot of dTTP and dGTP (200 μM final concentration) was added to initiate the elongation reaction. Aliquots of the reactions were quenched with EDTA at variable times and analyzed by denaturing gel electrophoresis to assess elongation. Representative gel electrophoresis data provided in Figure 5B shows that pol η effectively performs pro-mutagenic DNA synthesis when replicating 8-oxo-G as it easily extends beyond either dCMP and dAMP when paired opposite 8-oxo-G. An interesting feature is that pol η can elongate one base beyond dAMP even in the absence of the next correct nucleotide. Furthermore, pol η easily extends beyond the dAMP mispair to yield full length product when supplied with the correct nucleotides needed for elongation.

Pol η also efficiently extends beyond most of the modified nucleotides substrates tested here when paired opposite 8-oxo-G. Similar to what was observed for the elongation of the dAMP:8-oxo-G mispair, pol η extends beyond these modified purines, even in the absence of the next correct nucleotide. However, slight differences are observed in the efficiency of elongation when supplied with nucleotides needed for complete elongation of the primer. For example, the halogenated analog, 6-Cl-PTP is elongated with a higher efficiency compared to either of the alkylated nucleotides, N^6-MedATP and O^6-MedGTP. Surprisingly, pol η incorporates 6-NITP opposite 8-oxo-G and subsequently extends it one base pair in the absence of complementary dNTPs. However, pol η poorly extends beyond the non-natural nucleotide when supplied with dTTP and dGTP. This later result is consistent with previous reports demonstrating that high-fidelity DNA polymerases have severe difficulties in elongating substituted 5- and 6-nitroindolyl-nucleotides (26).

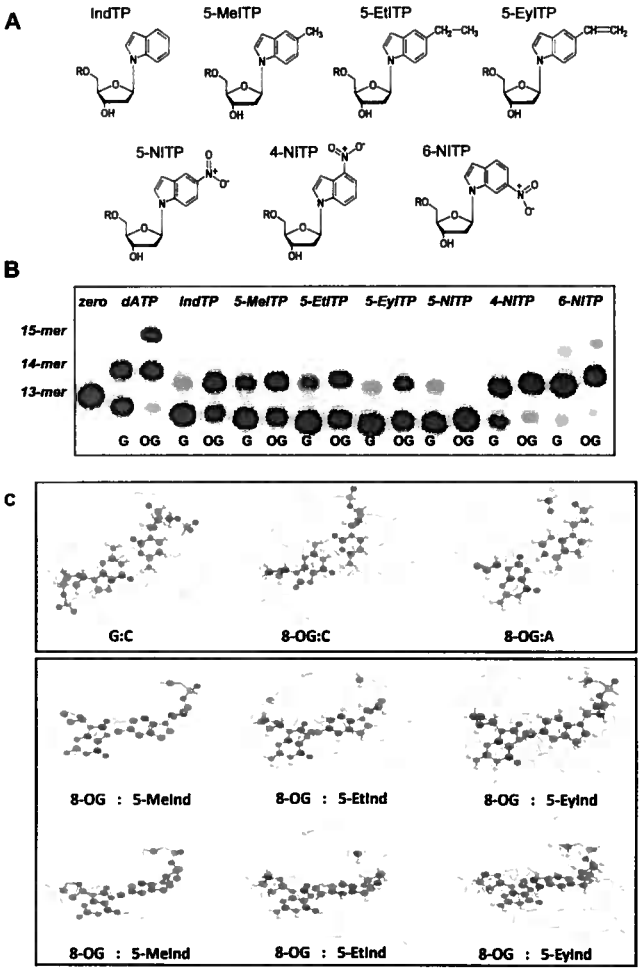

Figure 4. (**A**) Structures of non-natural nucleotides used in this study. (**B**) Gel electrophoresis data comparing the incorporation of non-natural nucleotides opposite G and 8-oxo-G catalyzed by pol η. (**C**) The top panel provides molecular models comparing the structures of basepairs between G : C, 8-oxo-G : C and 8-oxo-G : A. The bottom panel provides molecular models comparing the structures of basepairs between non-natural nucleotides paired opposite 8-oxo-G. The left panel provides models for 5-MeInd paired opposite 8-oxo-G (top and side view). The middle panel provides models for 5-EtInd paired opposite 8-oxo-G (top and side view). The right panel provides models for 5-EyInd paired opposite 8-oxo-G (top and side view).

Perhaps the most unusual behavior is again exhibited by N^2-MedGTP as pol η efficiently inserts N^2-MedGTP opposite 8-oxo-G and continues to elongate the mispair in the absence of complementary dNTP. This is highly unusual as pol η effectively misinserts N^2-MedGMP opposite a templating A (position 15) before inserting N^2-MedGTP opposite two templating C bases (positions 16 and 17). The ability of pol η to efficiently extend beyond 8-oxo-G again highlights the pro-mutagenic behavior of this alkylated nucleotide. It should be noted that this type of pro-mutagenic synthesis is highly selective for replication of the oxidized DNA lesion as pol η poorly incorporates and elongates N^2-MedGMP when replicating undamaged G.

DISCUSSION

Mutagenesis is defined as the inappropriate change in an organism's genomic information. This process is influenced by a number of cellular factors including the number and diversity of DNA lesions that can form after exposure to DNA damaging agents. For example, hyperoxic conditions present in organs such as the lung can generate ROS which in turn can produce a number of distinctive DNA lesions. If left unrepaired, these lesions can be misreplicated by various DNA polymerases, and the resulting mutations that arise can significantly increase the risk of initiating cancer.

To better understand how misreplicating damaged DNA influences cancer initiation and progression, we evaluated the ability of high-fidelity and specialized DNA polymerases to replicate 8-oxo-G, a DNA lesion that is commonly formed by ROS. Our results validate that 8-oxo-G is a pro-mutagenic DNA lesion as dAMP is efficiently inserted opposite the lesion by several different DNA polymerases. In the case of high-fidelity DNA polymerases, the efficiency for inserting dAMP is only 5-fold lower than that for inserting dCMP, the correct pairing partner for 8-oxo-G. This reduced fidelity contrasts what is observed during the replication of undamaged DNA in which the efficiency for dCMP incorporation opposite G is 10^6-fold higher than the misincorporation of dAMP. At face value, the reduced fidelity for replicating 8-oxo-G suggests that high fidelity polymerases are primarily responsible for misreplicating this oxidized lesion under cellular conditions. However, the kinetic data presented here suggests an alternative model in which the activity pol η plays a more important role in the pro-mutagenic behavior of 8-oxo-G. This model is predicated on the fact that high-fidelity DNA polymerases display remarkable low catalytic efficiencies for inserting either dAMP or dCMP opposite 8-oxo-G ($\sim 10^3$ $M^{-1}s^{-1}$) compared to normal DNA synthesis ($\sim 10^6$ $M^{-1}s^{-1}$). As outlined in Figure 6, the reduced efficiency for replicating 8-oxo-G would likely stall pol δ at the oxidized base, and this would facilitate polymerase switching to allow the specialized polymerase, pol η, to replace its more faithful counterpart. This is consistent with work published by Markkanen *et al.* (43) demonstrating that pol δ stalls at 8-oxo-G and is replaced with pol λ, another specialized DNA polymerase. While this group showed that pol λ promotes error free bypass of 8-oxo-G, the kinetic data presented here indicates that pol η can also by-pass 8-oxo-G as it is also more efficient at replicating the oxidized lesion than pol δ (compare 10^4 $M^{-1}s^{-1}$ versus 10^3 $M^{-1}s^{-1}$). Furthermore, the catalytic efficiencies measured for pol η inserting either dCMP or dAMP opposite 8-oxo-G are nearly identical, and this equality predicts that pol η will misreplicate 8-oxo-G with a relatively high frequency of ~50%. This is a significantly higher frequency compared to pol δ which is predicted to correctly insert dCMP about 80% of the time. These differences in replication efficiencies and fidelity are predicted to favor the ability of pol η to replicate 8-oxo-G in an error-prone manner under cellular conditions causing an increase in mutagenic events associated with diseases such as cancer. Several recent reports support this potential mechanism. For example, higher pol η expression correlates with poor outcomes in patients with non-small-cell lung cancer (44).

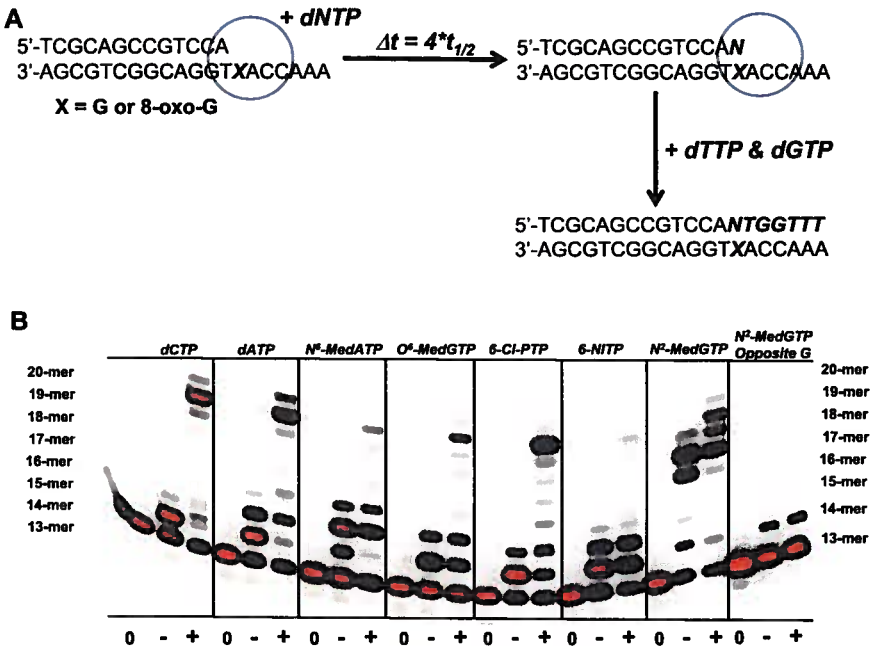

Figure 5. (**A**) Protocols used to measure insertion and extension beyond various nucleotides opposite 8-oxo-G. Assays were performed using single turnover reaction conditions in which pol η (500 nM) and 13/20OG-mer (250 nM) were pre-incubated and then mixed with a fixed concentration of nucleotide (dNTP) and 5 mM Mg^{2+}. After four half-lives, an aliquot of dTTP and dGTP (200 μM final concentration) was added to initiate the elongation reaction. Aliquots of the reactions were quenched with EDTA at variable times and analyzed by denaturing gel electrophoresis to assess elongation. (**B**) Representative gel electrophoresis data comparing the ability of pol η to extend beyond various mispairs containing 8-oxo-G. See text for further details.

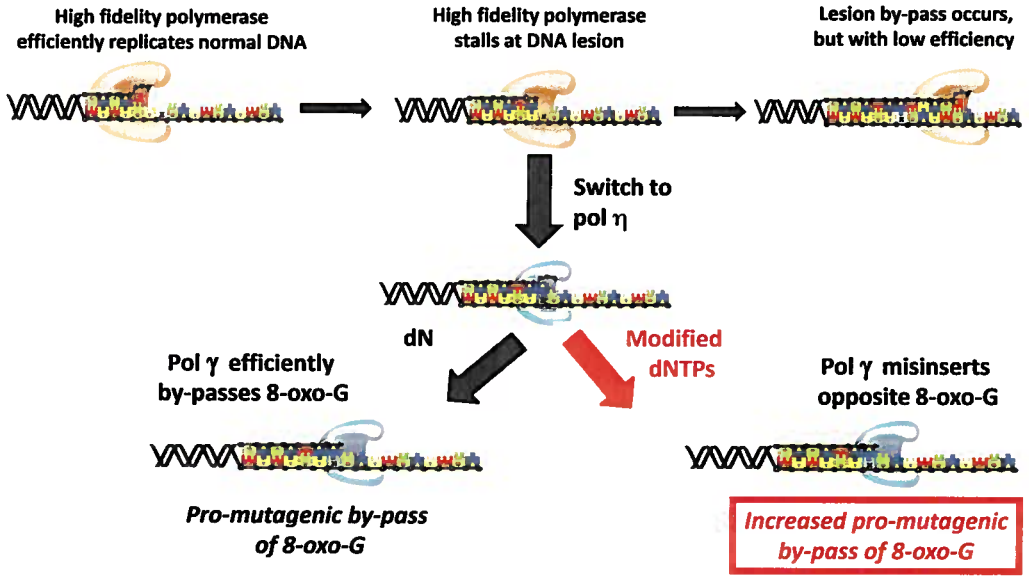

Figure 6. Hypothetical model for the coordination of pol δ and pol η activity during the replication of damaged DNA. In this model, pol δ stalls upon encountering the oxidized DNA lesion. Stalling would facilitate polymerase switching and allow pol η to replace pol δ. pol η is more efficient at misinserting dAMP opposite 8-oxo-G, and this predicts an increase in promutagenic replication. In addition, certain modified nucleotides including N^2-MedGTP are utilized more efficiently by pol η and are thus predicted to increase mutagenesis.

In particular, high expression of pol η is associated with shorter survival times in non-small cell lung cancer patients treated with platinum drugs (44). Finally, high levels of pol η correlate with resistance to chemotherapeutic agents such as cisplatin (45). In this case, drug resistance likely reflects the ability of pol η to incorporate nucleotides opposite and beyond the crosslinked lesion. In fact, *in vitro* studies have demonstrated that pol η can efficiently replicate cisplatinated DNA (46,47). Collectively, the results from our study demonstrate that pol η can efficiently replicate 8-oxo-G in an error-prone manner, and this offers new insights into how the activity of specialized DNA polymerases can contribute to cancer initiation and progression.

In addition, the kinetic data here show that certain modifications to the incoming nucleotide can significantly increase the frequency of mutagenic events catalyzed by pol η during TLS. The best example of this phenomenon is exhibited by N^2-MedGTP which is inserted opposite 8-oxo-G with a remarkably high catalytic efficiency compared to natural dNTPs. In particular, N^2-MedGTP is utilized ~10-fold more efficiently than either dATP or dCTP. Furthermore, N^2-MedGTP is surprisingly selective for insertion opposite 8-oxo-G compared to undamaged G. This is best illustrated by examining the ability of pol η to extend beyond mispairs containing N^2-MedGMP placed opposite 8-oxoG versus undamaged G (Figure 5B). As illustrated, pol η inserts and extends beyond N^2-MedGTP at least 1000-fold better when replicating the oxidized lesion compared to unmodified G. Collectively, the high efficiency for insertion opposite and extension beyond damaged DNA predicts that N^2-MedGTP is a highly pro-mutagenic nucleotide, especially when utilized by pol η during TLS. However, cell-based studies are clearly needed to verify that the kinetic phenomena described here can be recapitulated under cellular conditions.

Close inspection of the data summarized in Table 2 also points to an interesting trend in which nucleobase modifications have a more pronounced effect on the overall selectivity for incorporation opposite 8-oxo-G compared to G. For example, replacing a hydrogen bonding moiety such as the exocyclic amino group of dATP with a halogen (6-Cl-PTP) increases the efficiency of insertion opposite 8-oxo-G by ~8.5-fold compared to its insertion opposite G. Similar effects are observed with other analogs including N^6-MedATP (2.2-fold), O^6-MedGTP (17.2-fold) and N^2-MedGTP (41-fold) as all of these modified nucleotides show higher selectivity for incorporation opposite damaged DNA compared to normal DNA. Again, this change in selectivity results from specific nucleobase modifications as the natural substrate, dATP displays no selectivity for replicating damaged DNA as the catalytic efficiencies for insertion opposite normal G and 8-oxo-G are identical. Similar effects are observed for the incorporation of dGTP opposite the natural or oxidized nucleobase. The provocative implication of these results is that pol η uses different molecular mechanisms to replicate normal and damaged DNA. This may occur by the ability of pol η to use different biophysical features such as hydrogen-bonding interactions, shape complementarity and nucleobase hydrophobicity as a consequence of the physical nature of the templating base, i.e. normal versus damaged DNA.

To interrogate this potential mechanism, we performed molecular modeling studies that compare the predicted interactions of the natural substrate, dATP, in the active site of pol η with two modified nucleotides, N^2-MedGTP and 6-NITP. These particular nucleotides were chosen as they are incorporated opposite 8-oxo-G with higher catalytic efficiencies compared to dATP, and in the case of N^2-MedGTP, with increased selectivity for insertion opposite 8-oxo-G. The model provided in Figure 7A shows that dAMP interacts with 8-oxo-G in the *syn*-conformation and is mediated almost exclusively via hydrogen bonding interactions. This mode of interaction is consistent with structural data obtained from both high fidelity and specialized DNA polymerases that show nearly identical interactions between dAMP and the oxidized nucleobase (17,19,22). The model provided in Figure 7B shows the structure of the active site of pol η containing N^2-MedGMP paired opposite 8-oxo-G in the *syn* conformation. The major difference is that there are few, if any, direct hydrogen bonding interactions made between 8-oxo-G with the incoming alkylated nucleobase. In addition, the predicted interglycosyl distance between N^2-MedGMP and 8-oxo-G is slightly longer compared to that predicted for dAMP paired opposite 8-oxo-G (compare 9.2 Å versus 8.9 Å, respectively). While both features predict that N^2-MedGTP should be poorly incorporated opposite 8-oxo-G, our kinetic data demonstrate that the efficiency for utilizing N^2-MedGTP is almost an order of magnitude higher than dATP utilization. We propose that this increase in efficiency reflects favorable entropic contributions made between the hydrophobic methyl group of N^2-MedGTP with hydrophobic amino acids within the active site of pol η. Indeed, closer inspection of this model reveals the presence of a hydrophobic pocket that lines the back wall of the active site of pol η. Of particular importance are two isoleucine residues, Ile48 and Ile114, that exist within ~5 Å of the methyl group of N^2-MedGTP and could interact with the hydrophobic methyl group of N^2-MedGTP via van der Waals interactions. These entropic interactions may explain why the K_m of 0.64 μM for N^2-MedGTP is ~70-fold lower than the K_m of 47 μM measured for dATP. The model provided in Figure 7C showing the molecular interactions of 6-NITP with 8-oxo-G is consistent with this mechanism. As expected for this non-natural nucleoside, there are no hydrogen bonding contacts made between 6-NIMP with 8-oxo-G. However, the nitro group of 6-NIMP exists in a similar location as the methyl group of N^2-MedGTP. In fact, the model in Figure 7C shows that this hydrophobic nitro group is close to Ile48 and Ile114, and the close proximity could allow for favorable interaction with these hydrophobic amino acids through van der Waals contacts. Again, these favorable entropic interactions may explain why the measured K_m of 3.9 μM measured for 6-NITP is ~12-fold lower than that measured for dATP. It is interesting to note that the predicted distances between the nitro group of 6-NIMP and Ile48/Ile114 are longer than those measured between N^2-MedGTP and these hydrophobic amino acids, and this increase in distance may explain the differences in measure K_m values between the two modified nucleotides. In addition, the predicted interglycosyl distance between 6-NIMP and 8-oxo-G is 10 Å and slightly longer than those for an dAMP:8-oxo-G or N^2-Me-dGMP:8-oxo-G base pair. Thus,

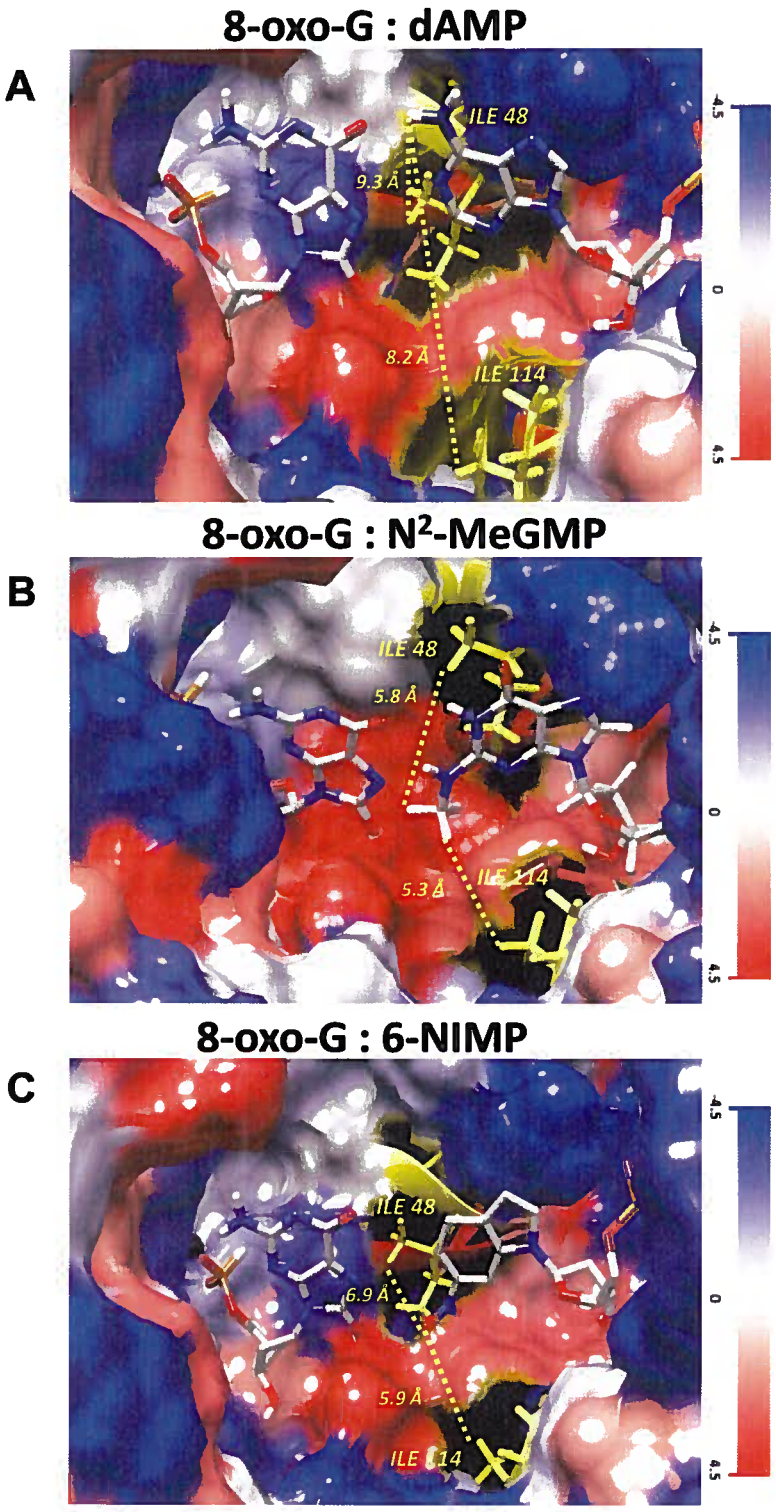

Figure 7. Molecular models of 8-oxo-G paired opposite dAMP (panel A), N^2-MedGMP (panel B), and 6-NIMP (panel C) in the active site of pol eta. These models were generated using molecular modeling programs, *MOE* and *Chimera*. The amino acid residues are color coded based on the Kyle Doolittle hydrophobicity scale, where blue denotes hydrophilic residues and red denotes hydrophobic residues. Ile114 and Ile48 are hydrophobic residues color coded in yellow for convenience. The close proximity of Ile114 and Ile48 (5–6 A^0) to the hydrophobic methyl group of N^2-MedGMP is proposed to play a key role in achieving an high catalytic efficiency ($1.7 * 10^5$ $M^{-1}s^{-1}$) for insertion opposite 8-oxo-G. Similarly, 6-NIMP with a nitro moiety at its sixth position is also inserted with a high efficiency ($7.26 * 10^4$ $M^{-1}s^{-1}$) opposite 8-oxo-G. This decrease could be attributed to a slight increase in distance between the nitro moiety and the isoleucine residues.

a lack of steric fit and shape complementarity might also explain the higher K_m value measure for 6-NITP compared to N^2-MedGTP.

This new information provides additional insight into to the mechanism by which pol η selects nucleotides when replicating damaged DNA. Current structural data of specialized DNA polymerases have produced two mutually exclusive mechanisms to account for their activities in replicating various DNA lesions. Compared to high-fidelity DNA polymerases which possess more constrained active sites, the active sites of specialized DNA polymerases such as pol η are enlarged such that they can accommodate structurally diverse DNA lesions, many of which are significantly larger and bulkier compared to undamaged nucleobases (34). Based on this difference, models invoking steric fit and shape complementarity are often used to explain the high efficiency displayed by pol η when replicating damaged DNA as well as its error-prone behavior when replicating undamaged DNA. However, structural studies also highlight an important role for hydrogen-bonding interactions. For example, the structure of pol η bound to a cisplatinated DNA lesion shows that dCTP properly pairs with the first templating nucleobase via conventional hydrogen bonding interactions (48). This result suggest that enthalpic contributions associated with forming Watson–Crick hydrogen bonds between the incoming nucleotide and templating base are the primary driving force for nucleotide utilization. Our kinetic data support a model for enthlapic contributions as modifications to hydrogen bonding groups present on the incoming dNTP tend to generate negative effects on their utilization by pol η during TLS.

FUNDING

Research was funded by the Department of Defense [W81XWH-13-1-0238 to A.J.B.] and the National Institutes of Health [RO1 GM13307 to S.J.B.].
Conflict of interest statement. None declared.

REFERENCES

1. Echols,H. and Goodman,M.F. (1991) Fidelity mechanisms in DNA replication. *Annu. Rev. Biochem.*, **60**, 477–511.
2. Kool,E.T. (2001) Hydrogen bonding, base stacking, and steric effects in DNA replication. *Annu. Rev. Biophys. Biomol. Struct.*, **30**, 1–22.
3. Kunkel,T.A. and Bebenek,K. (2000) DNA replication fidelity. *Annu. Rev. Biochem.*, **69**, 497–529.
4. Indiani,C., Langston,L.D., Yurieva,O., Goodman,M.F. and O'Donnell,M. (2009) Translesion DNA polymerases remodel the replisome and alter the speed of the replicative helicase. *Proc. Natl. Acad. Sci. U.S.A.*, **106**, 6031–6038.
5. Schärer,O.D. (2003) Chemistry and biology of DNA repair. *Angew Chem. Int. Ed. Engl.*, **42**, 2946–2974.
6. McCulloch,S.D. and Kunkel,T.A. (2008) The fidelity of DNA synthesis by eukaryotic replicative and translesion synthesis polymerases. *Cell Res.*, **18**, 148–161.
7. Maga,G., van Loon,B., Crespan,E., Villani,G. and Hübscher,U. (2009) The block of DNA polymerase delta strand displacement activity by an abasic site can be rescued by the concerted action of DNA polymerase beta and Flap endonuclease 1. *J. Biol. Chem.*, **284**, 14267–14275.
8. Zhong,X., Pedersen,L.C. and Kunkel,T.A. (2008) Characterization of a replicative DNA polymerase mutant with reduced fidelity and increased translesion synthesis capacity. *Nucleic Acids Res.*, **36**, 3892–3904.
9. O'Day,C.L., Burgers,P.M. and Taylor,J.S. (1992) PCNA-induced DNA synthesis past cis-syn and trans-syn-I thymine dimers by calf thymus DNA polymerase delta in vitro. *Nucleic Acids Res.*, **20**, 5403–5406.
10. Crespan,E., Amoroso,A. and Maga,G. (2010) DNA polymerases and mutagenesis in human cancers. *Subcell. Biochem.*, **50**, 165–188.
11. Hoffmann,J.S. and Cazaux,C. (2010) Aberrant expression of alternative DNA polymerases: a source of mutator phenotype as well as replicative stress in cancer. *Semin. Cancer Biol.*, **20**, 312–319.
12. Arana,M.E. and Kunkel,T.A. (2010) Mutator phenotypes due to DNA replication infidelity. *Semin. Cancer Biol.*, **20**, 304–311.
13. Asagoshi,K., Terato,H., Ohyama,Y. and Ide,H. (2002) Effects of a guanine-derived formamidopyrimidine lesion on DNA replication: translesion DNA synthesis, nucleotide insertion, and extension kinetics. *J. Biol. Chem.*, **277**, 14589–14597.
14. Wang,Z., Rhee,D.B., Lu,J., Bohr,C.T., Zhou,F., Vallabhaneni,H., de Souza-Pinto,N.C. and Liu,Y. (2010) Characterization of oxidative guanine damage and repair in mammalian telomeres. *PLoS Genet.*, **6**, e1000951.
15. Hsu,G.W., Ober,M., Carell,T. and Beese,L.S. (2004) Error-prone replication of oxidatively damaged DNA by a high-fidelity DNA polymerase. *Nature*, **431**, 217–221.
16. Beckman,J., Wang,M., Blaha,G., Wang,J. and Konigsberg,W.H. (2010) Substitution of ala for Tyr567 in RB69 DNA polymerase allows dAMP to be inserted opposite 7,8-dihydro-8-oxoguanine. *Biochemistry*, **49**, 4116–4125.
17. Brieba,L.G., Eichman,B.F., Kokoska,R.J., Doublie,S., Kunkel,T.A. and Ellenberger,T. (2004) Structural basis for the dual coding potential of 8-oxoguanosine by a high-fidelity DNA polymerase. *EMBO J.*, **23**, 3452–3461.
18. Zang,H., Irimia,A., Choi,J-Y., Angel,K.C., Loukachevitch,L.V., Egli,M. and Guengerich,F.P. (2006) Efficient and high fidelity incorporation of dCTP opposite 7,8-dihydro-8-oxodeoxyguanosine by *Sulfolobus solfataricus* DNA polymerase Dpo4. *J. Biol. Chem.*, **281**, 2358–2372.
19. Irimia,A., Eoff,R.L., Guengerich,F.P. and Egli,M. (2009) Structural and functional elucidation of the mechanism promoting error-prone synthesis by human DNA polymerase κ opposite the 7,8-dihydro-8-oxo-2′-deoxyguanosine adduct. *J. Biol. Chem.*, **284**, 22467–22480.
20. Carlson,K.D. and Washington,M.T. (2005) Mechanism of efficient and accurate nucleotide incorporation opposite 7,8-dihydro-8-oxoguanine by Saccharomyces cerevisiae DNA polymerase eta. *Mol. Cell Biol.*, **25**, 2169–2176.
21. McCulloch,S.D., Kokoska,R.J., Garg,P., Burgers,P.M. and Kunkel,T.A. (2009) The efficiency and fidelity of 8-oxo-guanine bypass by DNA polymerases delta and eta. *Nucleic Acids Res.*, **37**, 2830–2840.
22. Patra,A., Nagy,L.D., Zhang,Q., Su,Y., Müller,L., Guengerich,F.P. and Egli,M. (2014) Kinetics, structure, and mechanism of 8-Oxo-7,8-dihydro-2′-deoxyguanosine bypass by human DNA polymerase η. *J. Biol. Chem.*, **289**, 16867–16882.
23. Zhang,X., Lee,I. and Berdis,A.J. (2004) Evaluating the contributions of desolvation and base-stacking during translesion DNA synthesis. *Org. Biomol. Chem.*, **2**, 1703–1711.
24. Vineyard,D., Zhang,X., Donnelly,A., Lee,I. and Berdis,A.J. (2007) Optimization of non-natural nucleotides for selective incorporation opposite damaged DNA. *Org. Biomol. Chem.*, **5**, 3623–3630.
25. Motea,E.A., Lee,I. and Berdis,A.J. (2012) Development of a 'clickable' non-natural nucleotide to visualize the replication of non-instructional DNA lesions. *Nucleic Acids Res.*, **40**, 2357–2367.
26. Golden,J., Motea,E., Zhang,X., Choi,J.S., Feng,Y., Xu,Y., Lee,I. and Berdis,A.J. (2013) Development and characterization of a non-natural nucleoside that displays anticancer activity against solid tumors. *ACS Chem. Biol.*, **8**, 2452–2465.
27. Capson,T.L., Peliska,J.A., Kaboord,B.F., Frey,M.W., Lively,C., Dahlberg,M. and Benkovic,S.J.(1992) Kinetic characterization of the polymerase and exonuclease activities of the gene 43 protein of bacteriophage T4. *Biochemistry*, **31**, 10984–10994.
28. Hu,Z., Perumal,S.K., Yue,H. and Benkovic,S.J (2012). The human lagging strand DNA polymerase δ holoenzyme is distributive. *J. Biol. Chem.*, **287**, 38442–38448.
29. McCulloch,S.D., Kokoska,R.J., Chilkova,O., Welch,C.M., Johansson,E., Burgers,P.M. and Kunkel,T.A. (2004) Enzymatic

switching for efficient and accurate translesion DNA replication. *Nucleic Acids Res.*, **32**, 4665–4675.
30. Berdis,A.J. (2001) Dynamics of translesion DNA synthesis catalyzed by the bacteriophage T4 exonuclease-deficient DNA polymerase. *Biochemistry*, **40**, 7180–7191.
31. Johnson,R.E., Washington,M.T., Prakash,S. and Prakash,L. (2000) Fidelity of human DNA polymerase eta. *J. Biol. Chem.*, **275**, 7447–7450.
32. Matsuda,T., Bebenek,K., Masutani,C., Hanaoka,F. and Kunkel,T.A. (2000) Low fidelity DNA synthesis by human DNA polymerase-eta. *Nature*, **404**, 1011–1013.
33. Alt,A., Lammens,K., Chiocchini,C., Lammens,A., Pieck,J.C., Kuch,D., Hopfner,K.P. and Carell,T. (2007) Bypass of DNA lesions generated during anticancer treatment with cisplatin by DNA polymerase eta. *Science*, **318**, 967–970.
34. Zhao,Y., Biertümpfel,C., Gregory,M.T., Hua,Y.J., Hanaoka,F. and Yang,W. (2012) Structural basis of human DNA polymerase η-mediated chemoresistance to cisplatin. *Proc. Natl. Acad. Sci. U.S.A.*, **109**, 7269–7274.
35. Ummat,A., Rechkoblit,O., Jain,R., Roy Choudhury,J., Johnson,R.E., Silverstein,T.D., Buku,A., Lone,S., Prakash,L., Prakash,S. *et al.* (2012) Structural basis for cisplatin DNA damage tolerance by human polymerase η during cancer chemotherapy. *Nat. Struct. Mol. Biol.*, **19**, 628–632.
36. Brieba,L.G., Kokoska,R.J., Bebenek,K., Kunkel,T.A. and Ellenberger,T. (2005) A lysine residue in the fingers subdomain of T7 DNA polymerase modulates the miscoding potential of 8-oxo-7,8-dihydroguanosine. *Structure (Camb)*, **13**, 1653–1659.
37. Freudenthal,B.D., Beard,W.A. and Wilson,S.H. (2013) DNA polymerase minor groove interactions modulate mutagenic bypass of a templating 8-oxoguanine lesion. *Nucleic Acids Res.*, **41**, 1848–1858.
38. Yang,W. (2005) Portraits of a Y-family DNA polymerase. *FEBS Lett.*, **579**, 868–872.
39. Moran,S., Ren,R.X. and Kool,E.T. (1997) A thymidine triphosphate shape analog lacking Watson-Crick pairing ability is replicated with high sequence selectivity. *Proc. Natl. Acad. Sci. U.S.A.*, **94**, 10506–10511.
40. Fujiwara,S., Sawada,K. and Amisaki,T. (2014) Molecular dynamics study on conformational differences between dGMP and 8-oxo-dGMP: Effects of metal ions. *J. Mol. Graph Model.*, **51**, 158–167.
41. Zhang,X., Lee,I. and Berdis,A.J. (2005) The use of nonnatural nucleotides to probe the contributions of shape complementarity and pi-electron surface area during DNA polymerization. *Biochemistry*, **44**, 13101–13110.
42. Motea,E.A., Lee,I. and Berdis,A.J. (2013) Insights into the roles of desolvation and π-electron interactions during DNA polymerization. *Chembiochem.*, **14**, 489–498.
43. Markkanen,E., Castrec,B., Villani,G. and Hübscher,U. (2012) A switch between DNA polymerases δ and λ promotes error-free bypass of 8-oxo-G lesions. *Proc. Natl. Acad. Sci. U.S.A.*, **109**, 20401–20406.
44. Zhou,W., Chen,Y.W., Liu,X., Chu,P., Loria,S., Wang,Y., Yen,Y. and Chou,K.M. (2013) Expression of DNA translesion synthesis polymerase η in head and neck squamous cell cancer predicts resistance to gemcitabine and cisplatin-based chemotherapy. *PLoS One.*, **8**, e83978.
45. Chen,Y.W., Cleaver,J.E., Hanaoka,F., Chang,C.F. and Chou,K.M. (2006) A novel role of DNA polymerase eta in modulating cellular sensitivity to chemotherapeutic agents. *Mol. Cancer Res.*, **4**, 257–265.
46. Vaisman,A., Masutani,C., Hanaoka,F. and Chaney,S.G. (2000) Efficient translesion replication past oxaliplatin and cisplatin GpG adducts by human DNA polymerase eta. *Biochemistry*, **39**, 4575–4580.
47. Albertella,M.R., Green,C.M., Lehmann,A.R. and O'Connor,M.J. (2005) A role for polymerase eta in the cellular tolerance to cisplatin-induced damage. *Cancer Res.*, **65**, 9799–9806.
48. Alt,A., Lammens,K., Chiocchini,C., Lammens,A., Pieck,J.C., Kuch,D., Hopfner,K.P. and Carell,T. (2007) Bypass of DNA lesions generated during anticancer treatment with cisplatin by DNA polymerase eta. *Science*, **318**, 967–970.